



**National and Kapodistrian University of
Athens**

School of Science - Department of Physics

Section of Solid State Physics

Program of Postgraduate Studies “**Materials Physics**”

**Calculations of spin transport properties
on topological insulator surfaces
doped with magnetic defects**

Adamantia Kosma

Supervisor: Professor P. Mavropoulos

Athens 2018

Acknowledgements

First of all, I would like to thank my supervisor Prof. Phivos Mavropoulos for his enlightening guidance, untiring support, and constant inspiration throughout the preparation of this Master's Thesis. His door was always open for discussions about physics, as well as for any explanation I needed regarding theoretical models studied in the course of this study. His high standards were decisive for the quality of this work.

I am deeply thankful to Prof. Nikolaos Stefanou for his willingness to devote time on assessing this thesis, as one of committee members, for fruitful discussions about Solid State Physics, and his valuable advices for scientific aspects.

I am grateful to Prof. Yuriy Mokrousov for his willingness to examine this thesis, as one of committee members, as well as for our discussions about my thesis project during my visit in Jülich.

I am particularly grateful to Dr. Philipp Rößmann for his endless willingness on helping me with any scientific or computational issue that came up.

I want to thank Prof. Stefan Blügel for giving me the opportunity to visit the Institute for Advanced Simulation: Quantum Theory of Materials (IAS-1).

Special thanks to my office mate Petros-Andreas Pantazopoulos for our scientific and non-scientific discussions.

I would like to thank the Institute for Advanced Simulation: Quantum Theory of Materials (IAS-1), Forschungszentrum Jülich for financing and hosting a two-week scientific visit during the preparation of this thesis.

Last but not least, i would like to thank my parents Marina and Nikos, my brother Dimitris, and my friends for their help and unlimited support that they provide to me.

This work was supported by computational time granted from the Greek Research & Technology Network (GRNET) in the National HPC facility - ARIS - under project ID pr00504.thin-TopMag.

Contents

Introduction	1
1 KKR Green function method	3
1.1 Definition of the Green function	3
1.2 Voronoi construction	4
1.3 Scattering theory	5
1.3.1 Single scattering theory	5
1.3.2 Multiple scattering theory	7
1.4 Scalar-relativistic approximation	8
1.5 Spin orbit coupling	9
1.6 Scattering off impurities	10
1.6.1 Green function of a crystal with impurities	10
1.6.2 Transition Rate	11
2 Impurity-driven spin-orbit torques	13
2.1 Spin-orbit torques	13
2.1.1 Kubo formalism	14
2.2 KKR Representation of Operators	15
2.2.1 Spin expectation value	15
2.2.2 Torque expectation value	16
2.2.3 Spin flux expectation value	16
2.3 Boltzmann formalism for the spin-orbit torque	17
2.3.1 Boltzmann transport equation	17
2.3.2 Response tensors in Boltzmann formalism	21
3 Spin-orbit torque in magnetically doped topological insulator surfaces	23
3.1 Introduction to topological insulators	23
3.2 Studied system: Bi_2Te_3 with Mn defects	24
3.3 Scattering due to magnetic Mn defects	26
3.4 Calculations of the response tensors based on Boltzmann formalism	34
4 Conclusion	37
Appendix	39
Bibliography	41

Introduction

The field of spintronics aims at a manipulation of the electron spin degree of freedom with applications in information technology. In recent years, it has been realized that the spin-orbit interaction in materials can affect their electronic properties in exotic ways that can be used in spintronics applications. There is a number of directions in spintronics that have emerged as a consequence. In this thesis we focus on the materials class of topological insulators [1] and on the effect of spin-orbit torque (SOT) .

Spin-orbit torques are a class of magnetic torques that rely on the transfer of angular momentum from the crystal lattice to the magnetization of magnetic defects, in the presence of an electric field. As it is shown in Fig. 1, the magnetization of a ferromagnetic layer on a substrate of strong spin-orbit coupling is rotated in response to an electrical current in the system, until finally the magnetization has acquired an opposite orientation. This spin precession by SOT is pivotal for an electric-field control of magnetic memory, where the “up” or “down” direction of magnetization is interpreted as a memory bit, while the SOT serves as a switching lever.

The phenomenon has been intensively studied the last years for ferromagnetic bilayers [2–4], i.e. systems of a thin ferromagnetic layer, which is deposited on top of a heavy metal substrate. The conclusion of these studies was that SOT can lead to the reversal of the magnetization in such systems.

In this thesis, the same effect will be investigated in a different system. We will study the spin-orbit torque on states of magnetic Mn defects, which are embedded in the surface of the topological insulator Bi_2Te_3 , and for which it has been found that they present ferromagnetic behavior in small concentrations. The topological insulator is chosen as a substrate, due to its special characteristics. Topological insulators are narrow-gap semiconductors in the bulk and conducting at the surface, i.e., they are characterized by metallic surface states. Consequently, all current flows near the surface, where the SOT effect takes place, without energy loss from Joule heating in the bulk. In addition, these surface states are special in the sense of their spin texture, due to strong spin-orbit coupling. Their spin polarization is directly mainly in the plane of the surface, while the magnetization of the Mn magnetic impurity atoms is perpendicular to the surface. As a result, the torque is maximized, since it depends on the cross product of the two quantities. Due to these properties, when the topological insulator surface is doped with Mn magnetic impurities, a strong current-induced spin-orbit torque is expected to act on the Mn impurity atoms.

This thesis is structured as follows.

In Chapter 1, the KKR (Korringa-Kohn-Rostoker) Green function method is presented.

More specifically, after a short definition of the Green function, we give an analysis of the single scattering theory and then we generalize this theory in case of the scattering by all atoms within the crystal, solving the multiple scattering problem in KKR representation. Based on the KKR method, we focus on the scattering problem of impurity atoms in otherwise periodic crystal, calculated the Green function of this system and scattering properties, such as the transition rate.

In Chapter 2, the physical meaning of the spin-orbit torques is introduced, initially, since its linear response to an applied electric field, based on the Kubo formalism. Furthermore, the expressions of the expectation values of the spin, of the torque and of the spin flux operators are given in KKR representation. Then, we show how the impurity-driven spin-orbit torque response tensors in an applied electric field can be calculated, using the Boltzmann transport formalism.

Applying the KKR Green function method and the Boltzmann formalism we calculate the spin-orbit torque for the states on the Fermi surface of the topological insulator Bi_2Te_3 at the impurity atom Mn in Chapter 3. At first, the topological insulators and the special characteristics of their surface states are briefly introduced. Then, we discuss about the studied system, a Bi_2Te_3 surface doped with magnetic Mn defects. Finally, we present the results and discussion of our calculations of spin-orbit torque, spin-accumulation and spin flux in Mn/ Bi_2Te_3 system.

This thesis concludes in Chapter 4, where the results of our study are given in summary.

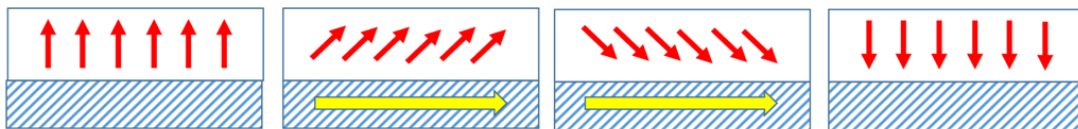


Figure 1: A schematic representation of the magnetic torque acting on a ferromagnetic layer on a substrate of strong spin-orbit coupling. The yellow and red arrows give the direction of the current \mathbf{j} and the magnetization, respectively.

Chapter 1

KKR Green function method

The calculation of the electronic structure of materials can be achieved by the KKR (Korringa-Kohn-Rostoker) function method, which was introduced by Korringa [5] and by Kohn and Rostoker [6]. This method was written as a wavefunction method, but it was reformulated as a Green function method [7–9], which is able to produce the crystal Green function by relating it to the Green function of free space via the Dyson equation. The KKR Green function method efficiently solves the multiple-scattering problem due to the presence of impurities within the crystal, which we will investigate in this thesis.

All first-principles calculations within this thesis was carried out with the KKRcode developed in Jülich, which is a full-potential relativistic implementation of the KKR Green function method method.

The development of the formalism in this Chapter is based on the Refs. [10–16].

1.1 Definition of the Green function

The Green operator for a system which is described by Hamiltonian H , is defined as

$$(E - H)G(E) = \mathbb{1} \quad (1.1)$$

In terms of eigenfunctions of H , $|\psi_i\rangle$, which obey the eigenvalues relation $H|\psi_i\rangle = \epsilon_i|\psi_i\rangle$, $G(E)$ can be obtained in the spectral representation of the green function in real space

$$G(\mathbf{x}, \mathbf{x}'; E) = \sum_i \frac{\psi_i(\mathbf{x})\psi_i^\dagger(\mathbf{x}')}{E - \epsilon_i + i\Gamma}, \quad (1.2)$$

representing in the limit of $\Gamma \rightarrow 0^+$ an outgoing wave at \mathbf{x} with a source term at \mathbf{x}' .

From the Eq. (1.2) it follows that the imaginary part of G is related to spectrally- and space-resolved density of states $\rho(\mathbf{x}; E)$. Integrating in space and using the Dirac identity the spectral density of states is derived

$$n(E) = -\frac{1}{\pi}\text{ImTr}G(E) \quad (1.3)$$

1.2 Voronoi construction

In the KKR formalism the space is divided into atomic cells. The center of each cell is the nuclear position and they are constructed as convex polyhedra by a Voronoi procedure. In this way the calculation of the Green function is decomposed at first into a set of local problems, with each one solved independently. In a second step, all local solutions are connected, finding the full Green function of the crystal in this way. This decomposition is achieved by defining a real space vector \boldsymbol{x} as

$$\boldsymbol{x} = \boldsymbol{r} + \boldsymbol{R}_n, \quad (1.4)$$

where \boldsymbol{R}_n is a lattice vector and \boldsymbol{r} is locally defined only within the cell n , as shown in Fig. 1.1.

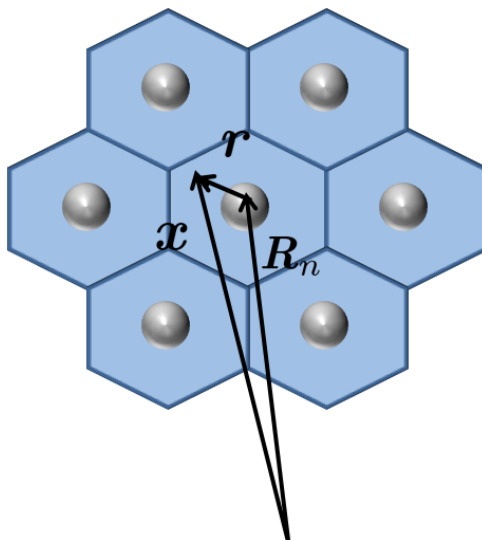


Figure 1.1: Illustration of the atomic cells found by Voronoi construction. In the center of the cells are shown the atoms of the crystal with gray color.

Within a crystal, the potential also must be cut off at the boundary of the atomic cells, using the shape function $\theta^n(\boldsymbol{r})$ [17]

$$\theta^n(\boldsymbol{r}) = \begin{cases} 1, & \text{if } \boldsymbol{r} + \boldsymbol{R}_n \in \text{cell } n \\ 0, & \text{otherwise,} \end{cases} \quad (1.5)$$

Then, the crystal potential is given by

$$V^n(\boldsymbol{r}) = V^n(\boldsymbol{r} + \boldsymbol{R}_n) \quad (1.6)$$

The shape functions are expanded into real spherical harmonics as

$$\theta^n(\boldsymbol{r}) = \sum_L \theta_L(r) Y_L(\hat{r}), \quad (1.7)$$

where we have used the combined index $L = \{l, m\}$ of the angular momentum indexes l and m .

In the systems studied in this thesis there are more than one atom per unit cell. In that case it is essential to define an additional vector $\boldsymbol{\chi}_\mu$, which determines the position of the μ th atom within a unit cell. The real space vector \boldsymbol{x} is written as

$$\boldsymbol{x} = \boldsymbol{r} + \boldsymbol{R}_n + \boldsymbol{\chi}_\mu \quad (1.8)$$

The crystal potential is then given by

$$V^{n\mu}(\boldsymbol{r}) = \begin{cases} V(\boldsymbol{r} + \boldsymbol{R}_n + \boldsymbol{\chi}_\mu), & \text{if } \boldsymbol{r} \in \text{cell } \{n, \mu\} \\ 0, & \text{otherwise} \end{cases} \quad (1.9)$$

1.3 Scattering theory

In this section the KKR multiple scattering method will be used for the solution of the Schrödinger equation. At first, we determine the scattering properties of each atom within the crystal. Second, we take into account the scattering events by all atoms, considering that the incident wave at each scattering center is equal to the sum of the outgoing waves from all other centers.

1.3.1 Single scattering theory

In a first step we will study the single scattering theory. We consider the scattering problem of a finite range atomic potential embedded in free space, of which the solutions are analytically known. The Green function of a free-electron system is given as [18]:

$$g(\boldsymbol{r}, \boldsymbol{r}'; E) = -\frac{e^{i\sqrt{E}|\boldsymbol{r}-\boldsymbol{r}'|}}{4\pi|\boldsymbol{r}-\boldsymbol{r}'|} \quad (1.10)$$

$$= \frac{1}{rr'} \sum_L Y_L(\hat{r}) g_l(\boldsymbol{r}, \boldsymbol{r}'; E) Y_L(\hat{r}') \quad (1.11)$$

In Eq. (1.11) the green function is written in angular momentum representation, which is a useful form for further calculations on scattering by a central potential. The expansion coefficients of Green function $g_l(\boldsymbol{r}, \boldsymbol{r}'; E)$ which introduced in Eq. (1.11), are defined as

$$g_l(\boldsymbol{r}, \boldsymbol{r}'; E) = \kappa r r' [\theta(r' - r) j_l(\kappa r) h_l(\kappa r') + \theta(r - r') h_l(\kappa r) j_l(\kappa r')], \quad (1.12)$$

where $j_l(\kappa r)$ are the Bessel functions and $h_l(\kappa r)$ are the Hankel functions, with $\kappa = \sqrt{E}$. The eigenfunctions in the case of free space, $\varphi_{\boldsymbol{k}}(\boldsymbol{r})$, are an incoming plane wave

$$\varphi_{\boldsymbol{k}}(\boldsymbol{r}) = e^{i\boldsymbol{k}\boldsymbol{r}} \quad (1.13)$$

$$= \sum_L 4\pi i^l j_l(\sqrt{E}r) Y_L(\hat{r}) Y_L(\hat{k}), \quad (1.14)$$

Supposing now, that there is a perturbed potential $V(\boldsymbol{r})$ of finite range embedded in free space, the eigenfunctions of the corresponding Hamiltonian yield the following Lippmann-Schwinger equation

$$\psi_{\boldsymbol{k}}^s(\boldsymbol{r}) = e^{i\boldsymbol{k}\boldsymbol{r}} \chi^s + \int d\boldsymbol{r}' g(\boldsymbol{r}, \boldsymbol{r}'; E_{\boldsymbol{k}}) V(\boldsymbol{r}') \psi_{\boldsymbol{k}}^s(\boldsymbol{r}'), \quad (1.15)$$

where $E_{\mathbf{k}} = k^2$ is the energy of a free particle of wave vector \mathbf{k} and χ^s is a spin state.

The Green function of this scattering problem is given in terms of the corresponding right regular $R_L(\mathbf{r})$ (converging at $r \rightarrow \infty$) and irregular $S_L(\mathbf{r})$ (diverging at $r \rightarrow 0$), since in terms of left regular $\bar{R}_L(\mathbf{r})$ and irregular $\bar{S}_L(\mathbf{r})$ scattering solutions

$$G_s(\mathbf{r}, \mathbf{r}'; E) = \kappa \sum_L [\theta(r' - r)R_L(\mathbf{r})\bar{S}_L(\mathbf{r}) + \theta(r - r')S_L(\mathbf{r})\bar{R}_L(\mathbf{r}')] \quad (1.16)$$

Expanding the wavefunctions in real spherical harmonics and replacing that in Eq. (1.15), we obtain the Lippmann-Schwinger equations which yield the scattering solutions:

$$R_L^s(\mathbf{r}; E) = j_l(\kappa r)Y_L(\hat{r})\chi^s + \int d\mathbf{r}' g(\mathbf{r}, \mathbf{r}'; E_{\mathbf{k}})V(\mathbf{r}')R_L^s(\mathbf{r}'; E) \quad (1.17)$$

$$S_L^s(\mathbf{r}; E) = \sum_{L'} h_{l'}(\kappa r)Y_{L'}(\hat{r})\beta_{LL'}^s(E) + \int d\mathbf{r}' g(\mathbf{r}, \mathbf{r}'; E_{\mathbf{k}})V(\mathbf{r}')S_L^s(\mathbf{r}'; E), \quad (1.18)$$

with β matrix

$$\beta_{LL'}^s(E) = \delta_{LL'}\chi^s - \kappa \int d\mathbf{r}' j_l(\kappa r)Y_L(\hat{r})V(\mathbf{r}')S_{L'}^s(\mathbf{r}'; E) \quad (1.19)$$

The scattering functions $R_L(\mathbf{r}), S_L(\mathbf{r})$ are called right solutions. On the other hand, the functions $\bar{R}_L(\mathbf{r}), \bar{S}_L(\mathbf{r})$ are referred as left solutions, since they obey a differential equation in which the Hamiltonian acts to the left-hand side, in the sense that is explained in Ref. [11]. These solutions are defined by similar Lippmann-Schwinger equations as right solutions. Both right and left solutions are expanded in real spherical harmonics:

$$R_L^s(\mathbf{r}; E) = \sum_{L'} \frac{1}{r} R_{L'L}^s(r; E) Y_{L'}(\hat{r}), \quad (1.20)$$

$$\bar{R}_L^s(\mathbf{r}; E) = \sum_{L'} \frac{1}{r} \bar{R}_{LL'}^s(r; E) Y_{L'}(\hat{r}) \quad (1.21)$$

The expansion coefficients of right scattering solutions $R_{L'L}^s(r; E), S_{L'L}^s(r; E)$ are 2×1 spinors in Schrödinger-Pauli theory, or 4×1 spinors in Dirac theory. They are calculated by the following Lippmann-Schwinger equations in the Fredholm formulation [11]:

$$R_{L'L}^s(r; E) = J_L(r; E)\delta_{L'L}\chi^s + \sum_{L''} \int dr'' g_{l'}(r, r''; E)V_{L'L''}(r'')R_{L''L}^s(r''; E) \quad (1.22)$$

$$S_{L'L}^s(r; E) = H_L(r; E)\beta_{L'L}^s(E) + \sum_{L''} \int dr'' g_{l'}(r, r''; E)V_{L'L''}(r'')S_{L''L}^s(r''; E), \quad (1.23)$$

where β matrix is defined by the expression:

$$\beta_{L'L}^s(E) = \delta_{L'L}\chi^s - \kappa \int dr' J_L(r'; E) \sum_{L''} V_{L'L''}(r')S_{L''L}^s(r'; E) \quad (1.24)$$

Respectively, the expansion coefficients of left scattering solutions, which are 1×2 spinors in Schrödinger-Pauli theory, or 1×4 spinors in Dirac theory, are given according to following Lippmann-Schwinger relations:

$$\bar{R}_{LL'}^s(r; E) = \bar{J}_L(r; E)\delta_{L'L}\chi^s + \sum_{L''} \int dr'' \bar{R}_{L''L}^s(r''; E)V_{L''L'}(r'')g_{L'}(r'', r; E) \quad (1.25)$$

$$\bar{S}_{LL'}^s(r; E) = \bar{\beta}_{LL'}(E)\bar{H}_L(r; E) + \sum_{L''} \int dr'' \bar{S}_{L''L}^s(r''; E)V_{L''L'}(r'')g_{L'}(r'', r; E), \quad (1.26)$$

with $\bar{\beta}$ matrix:

$$\bar{\beta}_{LL'}^s(E) = \delta_{LL'}\chi^s - \kappa \int dr' \bar{R}_{LL''}^s(r'; E) \sum_{L''} V_{L''L'}(r')H_{L'}(r'; E) \quad (1.27)$$

In the above relations we have used the abbreviations $J_L(r; E) = rj_l(\sqrt{E}r)$ and $H_L(r; E) = rh_l(\sqrt{E}r)$.

It is significant to introduce a fundamental quantity of scattering theory, the atomic transition matrix (t -matrix), which contains the scattering properties of the above system. Having calculated the regular scattering solutions, the Δt matrix is written as an integral

$$t_{LL'}(E) = \sum_{L''} \int dr \bar{J}_L(r; E)V_{LL''}^n(r)R_{L''L'}(r; E), \quad (1.28)$$

where $V^n(r)$ is the atomic potential on site n .

1.3.2 Multiple scattering theory

Until here we discussed the problem of an isolated scatterer. Having solved this, we will take into account the multiple scattering by all atoms within the crystal.

The expansion coefficients of the potential-free Green function, also called structure constants, of multiple scattering problem are given by the relation

$$g_{LL'}^{nn'} = -(1 - \delta_{nn'})4\pi\sqrt{E} \sum_{L''} i^{l-l'+l''} C_{LL'L''} h_{L''}(\mathbf{R}_n - \mathbf{R}_{n'}; E), \quad (1.29)$$

where we have used the Gaunt coefficients $C_{LL'L''} = \int d\Omega Y_L(\hat{r})Y_{L'}(\hat{r})Y_{L''}(\hat{r})$.

Assuming now, a scattering periodic potential in crystal, the Green function consists of two terms, the single-site term and the multiple scattering term, which refers to scatterers on different sites [19]

$$G(\mathbf{r} + \mathbf{R}_n, \mathbf{r}' + \mathbf{R}_{n'}; E) = \delta_{nn'}G_s(\mathbf{r}, \mathbf{r}'; E) + \sum_{\Lambda\Lambda'} R_{\Lambda}(\mathbf{r}; E)G_{\Lambda\Lambda'}^{nn'}(E)\bar{R}_{\Lambda'}(\mathbf{r}'; E) \quad (1.30)$$

In the above equation (1.30) the multi-index $\Lambda = (L, s) = (l, m, s)$ was introduced, which consists of the orbital and spin quantum numbers. The coefficients $G_{\Lambda\Lambda'}^{nn'}(E)$ are called structural Green functions and they can be determined by the following algebraic Dyson equation

$$G_{\Lambda\Lambda'}^{nn'}(E) = g_{\Lambda\Lambda'}^{nn'}(E) + \sum_{n''\Lambda''\Lambda'''} g_{\Lambda\Lambda''}^{nn''}(E) \Delta t_{\Lambda''\Lambda'''}^{n''}(E) G_{\Lambda''\Lambda'}^{n''n'}(E) \quad (1.31)$$

Expanding the sum on the right-hand side of Eq. (1.31), it is obvious that an electron can travel from site n' to n directly, or after scattering by the potential on site n , or n and n' , etc.

As we referred in section (1.2), the unit cell of the study system consists of more than one atoms per unit cell. In the next relations, we will introduce the index μ , taking into account the different atom types.

In practice, the calculations of Green functions are performed firstly in \mathbf{k} -space. The structural Green functions $g_{\Lambda\Lambda'}$ and $G_{\Lambda\Lambda'}$ are solved by matrix inversion after a cutoff at $l = l_{\max}$ ¹. We will introduce the Fourier transform of the structure constants $g_{\Lambda\Lambda'}^{\mu\mu'}(\mathbf{k}; E)$, which depends only on the geometry of the lattice and is given according to

$$g_{\Lambda\Lambda'}^{\mu\mu'}(\mathbf{k}; E) = \sum_{n'\mu'} g_{\Lambda\Lambda'}^{n\mu;n'\mu'}(E) e^{i\mathbf{k}\cdot(\mathbf{R}_n + \boldsymbol{\chi}_\mu - \mathbf{R}_{n'} - \boldsymbol{\chi}_{\mu'})} \quad (1.32)$$

Having calculated the structure constants and the t -matrix the eigenvalue problem can be solved for electrons in a periodic crystal. In particular, the bandstructure $E(\mathbf{k})$ of the crystal can be found by the KKR secular equation

$$\sum_{\Lambda'\mu'} \left[\delta_{\Lambda\Lambda'} \delta_{\mu\mu'} - \sum_{\Lambda''} g_{\Lambda\Lambda''}^{\mu\mu'}(\mathbf{k}; E) \Delta t_{\Lambda''\Lambda'}^{\mu'\mu}(E) \right] c_{\mathbf{k}\Lambda'}^{\mu'} = 0, \quad (1.33)$$

which gives for certain \mathbf{k} the corresponding energy E . The coefficients $c_{\mathbf{k}\Lambda}^{\mu'}$ are the eigenvectors for the total incoming wave at the scatterer on the site $\chi_{\mu'}$. These coefficients vectors correlate the Bloch wavefunctions in the crystal $\psi_{\mathbf{k}}$ with the radial scattering solutions R_{Λ}^{μ}

$$\psi_{\mathbf{k}}(\mathbf{r} + \mathbf{R}_n + \boldsymbol{\chi}_\mu) = \sum_{\Lambda} c_{\mathbf{k}\Lambda}^{\mu} R_{\Lambda}^{\mu}(\mathbf{r}; E) \quad (1.34)$$

1.4 Scalar-relativistic approximation

In this section we will include to our study relativistic effects. The scalar-relativistic approximation (SRA) neglects the spin-orbit coupling, keeping other relativistic effects. The motivation, then, of formulated this approximation is retaining spin as a good quantum number. We will generalize the single scattering problem of a finite range potential, which is described on Section 1.3.1 in the case of the scalar-relativistic approximation.

The potential-free Green function for the single-site scalar-relativistic approximation reads

$$\underline{\underline{G}}_l^0 = 2M_0\kappa\theta(r' - r)\underline{\underline{R}}_l^0(r)\underline{\underline{S}}_l^0(r') + 2M_0\kappa\theta(r - r')\underline{\underline{S}}_l^0(r)\underline{\underline{R}}_l^0(r'), \quad (1.35)$$

where we defined the relativistic mass M_0 and the momentum vector κ according to relations

$$M_0 \equiv \frac{1}{2} + \frac{E}{2c^2}, \quad \kappa = \sqrt{E + \frac{E^2}{c^2}} = \sqrt{2M_0E} \quad (1.36)$$

¹The l_{\max} is determined as the l after which the t matrix becomes negligible. In our calculations we used $l_{\max}=3$.

The regular and irregular right- and left-hand side potential free-solutions in scalar-relativistic approximation are given by:

$$\underline{R}_l^0(r) = r \left(\begin{array}{c} j_l(\kappa r) \\ \frac{1}{2M_0} \partial_r j_l(\kappa r) \end{array} \right), \quad \bar{R}_l^0(r) = r (j_l(\kappa r) - \frac{1}{2M_0} \partial_r j_l(\kappa r)) \quad (1.37)$$

$$\underline{S}_l^0(r) = r \left(\begin{array}{c} h_l(\kappa r) \\ \frac{1}{2M_0} \partial_r h_l(\kappa r) \end{array} \right), \quad \bar{S}_l^0(r) = r (h_l(\kappa r) - \frac{1}{2M_0} \partial_r h_l(\kappa r)) \quad (1.38)$$

The regular and irregular scattering solutions in the case of a finite potential in crystal can be calculated by Lippmann-Schwinger equations. Expanding the solutions in real spherical harmonics and replacing the potential-free single-site Green function (Eq. (1.35)) we arrive at the Lippmann-Schwinger equations in the Fredholm formulation, which yields the expansion coefficients of regular $\underline{R}_{LL'}(r; E)$ and irregular $\underline{S}_{LL'}(r; E)$ right-hand solutions [11]

$$\begin{aligned} \underline{R}_{LL'}(r; E) &= \underline{R}_L^0(r; E) \delta_{LL'} \\ &+ 2M_0 \kappa \underline{R}_L^0(r; E) \int_r^{R^{max}} dr' \bar{S}_L^0(r'; E) \sum_{L''} \Delta V_{\underline{LL}''}(r') \underline{R}_{L''L'}(r'; E) \\ &+ 2M_0 \kappa \underline{S}_L^0(r; E) \int_0^r dr' \bar{R}_L^0(r'; E) \sum_{L''} \Delta V_{\underline{LL}''}(r') \underline{R}_{L''L'}(r'; E) \end{aligned} \quad (1.39)$$

$$\begin{aligned} \underline{S}_{LL'}(r; E) &= \underline{S}_L^0(r; E) \beta_{LL'} \\ &+ 2M_0 \kappa \underline{R}_L^0(r; E) \int_r^{R^{max}} dr' \bar{S}_L^0(r'; E) \sum_{L''} \Delta V_{\underline{LL}''}(r') \underline{S}_{L''L'}(r'; E) \\ &+ 2M_0 \kappa \underline{S}_L^0(r; E) \int_0^r dr' \bar{R}_L^0(r'; E) \sum_{L''} \Delta V_{\underline{LL}''}(r') \underline{S}_{L''L'}(r'; E) \end{aligned} \quad (1.40)$$

where β is defined as

$$\beta_{LL'} = 1 + 2M_0 \kappa \int dr' \underline{R}_L^0(r') \sum_{L''} \Delta V_{\underline{LL}''}(r') \underline{S}_{L''L'}(r') \quad (1.41)$$

1.5 Spin orbit coupling

Spin-orbit coupling is the most important mechanism which couples the spin magnetic moment of an electron to its orbital angular momentum. This spin-orbit interaction is described by the Hamiltonian term

$$\hat{H}_{SO} = \frac{1}{M(r)^2} \frac{1}{c^2} \frac{\partial V(r)}{\partial r} \mathbf{L} \cdot \boldsymbol{\sigma}, \quad (1.42)$$

where $M(r)$ is the relativistic mass and c is the light velocity. The potential $V(r)$ is the average spin-up and spin-down potential, i.e. $V(r) = \frac{(V_{\uparrow} + V_{\downarrow})}{2}$.

Taking into account this interaction term, the problem is solved by the Pauli equation, which consists of the Schrödinger or the scalar-relativistic equations plus the spin-orbit

coupling Hamiltonian term. Then, the total Hamiltonian can be written as a 2×2 matrix in spin-space

$$\begin{pmatrix} H_{\uparrow\uparrow}^{tot} & H_{\uparrow\downarrow}^{tot} \\ H_{\downarrow\uparrow}^{tot} & H_{\downarrow\downarrow}^{tot} \end{pmatrix} = \begin{pmatrix} H_{\uparrow\uparrow} & 0 \\ 0 & H_{\downarrow\downarrow} \end{pmatrix} + \begin{pmatrix} H_{\uparrow\uparrow}^{SOC} & H_{\uparrow\downarrow}^{SOC} \\ H_{\downarrow\uparrow}^{SOC} & H_{\downarrow\downarrow}^{SOC} \end{pmatrix} \quad (1.43)$$

1.6 Scattering off impurities

The existence of an impurity or a defect in a periodic crystal will destroy its periodicity. The perturbing potential of the defects causes the multiple scattering of electrons in the crystal. This scattering problem can be solved in two steps. Firstly, we calculate the Green function of the crystal without impurities, and in a second step we calculate the effect of the impurities in the crystal, which is described by the perturbing potential ΔV .

1.6.1 Green function of a crystal with impurities

The atoms on the impurity region shall be labeled by a combined index $i = (n, \mu)$, where the center of the i th cell is located at

$$\boldsymbol{\tau}_i = \mathbf{R}_n + \boldsymbol{\chi}_\mu \quad (1.44)$$

Then, the real space vector which defined by Eq. (1.8) is given in form

$$\mathbf{x} = \mathbf{r} + \boldsymbol{\tau}_i \quad (1.45)$$

The calculation of the wavefunctions of an impurity $\psi_{\mathbf{k}}^{\text{imp}}(\mathbf{x})$, embedded in a periodic host system, has to be considered as a scattering problem. The scattering solutions of the impurity potential are related to the host eigenstates $\psi_{\mathbf{k}}(\mathbf{x})$ (Eq. 1.34) by the Lippmann-Schwinger equation

$$\psi_{\mathbf{k}}^{\text{imp}}(\mathbf{x}) = \psi_{\mathbf{k}}(\mathbf{x}) + \int d\mathbf{r}' G(\mathbf{x}, \mathbf{x}') \Delta V(\mathbf{x}') \psi_{\mathbf{k}}^{\text{imp}}(\mathbf{x}'), \quad (1.46)$$

where $G(\mathbf{x}, \mathbf{x}')$ is the Green function of the host system, which is calculated by Eq. (1.30) and $\Delta V(\mathbf{x}')$ is the perturbing potential in the host system, which is defined as the difference between the impurity potential and the potential of the host system, i.e. $\Delta V(\mathbf{x}') = V^{\text{imp}} - V^{\text{host}}$. We have to note that the host wavefunctions $\psi_{\mathbf{k}}(\mathbf{x})$ obey the Bloch's theorem, due to the periodicity of the crystal. In the calculations we choose usually another form of the Lippmann-Schwinger equation

$$\psi_{\mathbf{k}}^{\text{imp}}(\mathbf{x}) = \psi_{\mathbf{k}}(\mathbf{x}) + \int d\mathbf{r}' G^{\text{imp}}(\mathbf{x}, \mathbf{x}') \Delta V(\mathbf{x}') \psi_{\mathbf{k}}(\mathbf{x}'), \quad (1.47)$$

where is used the impurity Green function G^{imp} . This is consisted of two terms, the single-site term and the back-scattering term

$$G^{\text{imp}}(\mathbf{r} + \boldsymbol{\tau}_i, \mathbf{r}' + \boldsymbol{\tau}_{i'}) = \delta_{ii'} G_s^{\text{imp},i}(\mathbf{r}, \mathbf{r}') + \sum_{\Lambda\Lambda'} R_{\Lambda}^{\text{imp},i}(\mathbf{r}) G_{\Lambda\Lambda'}^{\text{imp},ii'} \bar{R}_{\Lambda'}^{\text{imp},i'}(\mathbf{r}') \quad (1.48)$$

The impurity scattering wavefunctions are expanded into the regular scattering solutions of the perturbed atomic potentials

$$\psi_{\mathbf{k}}^{\text{imp}}(\mathbf{r}) = \sum_{\Lambda} c_{\Lambda}^{\text{imp},i} R_{\Lambda}^{\text{imp},i}(\mathbf{r}; E) \quad (1.49)$$

The regular solutions are defined by the Lippmann-Schwinger equation

$$R_{\Lambda}^{\text{imp},i}(\mathbf{r}; E) = j_l(\kappa r) Y_L(\hat{r}) \chi^s + \int d\mathbf{r}' g(\mathbf{r}, \mathbf{r}'; E) V^{\text{imp}}(\mathbf{r}') R_{\Lambda}^{\text{imp},i}(\mathbf{r}'; E) \quad (1.50)$$

and they are expanded in real spherical harmonics according to

$$R_{\Lambda}^{\text{imp}}(\mathbf{r}; E) = R_L^{\text{imp},s}(\mathbf{r}; E) = \sum_{L'} \frac{1}{r} R_{L'L}^{\text{imp},s'}(\mathbf{r}; E) Y_{L'}(\hat{r}) \quad (1.51)$$

It can be proved that the coefficients $c_{\Lambda}^{\text{imp},i}$ are written in terms of the coefficients of the Bloch states $c_{\Lambda'}^{i'} = c_{\Lambda'}^{\mu'} e^{i\mathbf{k}\cdot\mathbf{R}_{n'}}$, i.e. of the host system states, according to relation [13]:

$$c_{\Lambda}^{\text{imp},i} = \sum_{\Lambda',i'} \left\{ \delta_{\Lambda\Lambda'} \delta_{ii'} + \sum_{\Lambda''} G_{\Lambda\Lambda''}^{\text{imp},ii'} \Delta t_{\Lambda''\Lambda'}^{\text{imp},i'} \right\} c_{\Lambda'}^{\mu'} e^{i\mathbf{k}\cdot\mathbf{R}_{n'}}, \quad (1.52)$$

where we have introduced the t-matrix elements, which are defined by

$$\Delta t_{\Lambda\Lambda'}^{\text{imp},i} = \sum_{\Lambda''\Lambda'''} \int dr \bar{R}_{\Lambda\Lambda''}^i(r) \Delta V_{\Lambda''\Lambda'''}^i(\mathbf{r}) R_{\Lambda'''\Lambda'}^{\text{imp},i}(r) \quad (1.53)$$

In addition, in Eq. (1.52) are used the matrix elements of the impurity Green function. The structural Green functions of the impurity are related to the structural Green functions of the host system by the algebraic Dyson equation

$$G_{\Lambda\Lambda'}^{\text{imp},ii'} = G_{\Lambda\Lambda'}^{\text{host},ii'} + \sum_{\Lambda''\Lambda'''} \sum_{i''} G_{\Lambda\Lambda''}^{\text{host},ii'} \Delta t_{\Lambda''\Lambda'''}^{i''} G_{\Lambda'''\Lambda'}^{\text{imp},i''i'}, \quad (1.54)$$

where $\Delta t_{\Lambda''\Lambda'''}^{i''} = t_{\Lambda''\Lambda'''}^{\text{imp},i''} - t_{\Lambda''\Lambda'''}^{\text{host},i''}$ is defined as the difference between the t-matrix of the impurity potential V^{imp} and the host potential V^{host} . The sum over the i'' is referred to atoms, for which the perturbation is significant. The Eq. (1.54) is solved in direct space with inversion matrix

$$G_{\Lambda\Lambda'}^{\text{imp},ii'} = [1 - G_{\Lambda\Lambda'}^{\text{host},ii'} \Delta t_{\Lambda''\Lambda'''}^{i''}]^{-1} G_{\Lambda\Lambda'}^{\text{host},ii'} \quad (1.55)$$

1.6.2 Transition Rate

An important quantity is being studied in scattering off impurities calculations is the transition rate $w_{\mathbf{k}\mathbf{k}'}$, which is defined as the scattering probability from an initial state \mathbf{k}' to a final state \mathbf{k} per unit time:

$$w_{\mathbf{k}\mathbf{k}'} = \frac{dP_{\mathbf{k}\mathbf{k}'}}{dt} \quad (1.56)$$

The knowledge of the transition rate between states leads to the calculation of measurable properties in solids such as relaxation time or transport properties, as we will discuss in Chapter 2. The scattering rate can be expressed in terms of the T -matrix by the Fermi's Golden Rule

$$w_{\mathbf{k}\mathbf{k}'} = \frac{2\pi}{\hbar} \delta(E(\mathbf{k}) - E(\mathbf{k}')) |T_{\mathbf{k}\mathbf{k}'}|^2, \quad (1.57)$$

The \mathbf{k} -space representation of the transition matrix is written as

$$T_{\mathbf{k}\mathbf{k}'} = \int d\mathbf{x} \psi_{\mathbf{k}'}^\dagger(\mathbf{x}) \Delta V(\mathbf{x}) \psi_{\mathbf{k}}^{\text{imp}}(\mathbf{x}) \quad (1.58)$$

Replacing in Eq. (1.58) the expansions of the host and impurity wavefunctions, according to equations (1.34) and (1.49) respectively, we arrive in another form of the scattering amplitudes

$$T_{\mathbf{k}\mathbf{k}'} = \sum_{\Lambda\Lambda'} \sum_i [c_{\mathbf{k}',\Lambda}^i]^* \Delta_{\Lambda\Lambda'}^i [c_{\mathbf{k},\Lambda'}^{\text{imp},i'}], \quad (1.59)$$

where the Δ -matrix reads [14]

$$\Delta_{\Lambda\Lambda'}^i = \sum_{\Lambda''\Lambda'''} \int d\mathbf{r} [R_{\Lambda\Lambda''}^i(\mathbf{r})]^* \Delta V_{\Lambda''\Lambda'''}^i(\mathbf{r}) R_{\Lambda''\Lambda'}^{\text{imp},i}(\mathbf{r}) \quad (1.60)$$

We can simplify the above equation (1.59) introducing the coefficients of the scattering wavefunction by Eq. (1.52), resulting in a form of the T -matrix in which only the coefficients of the Bloch states enter

$$T_{\mathbf{k}\mathbf{k}'} = \sum_{\Lambda\Lambda'} \sum_{i,i'} [c_{\mathbf{k}',\Lambda}^i]^* T_{\Lambda\Lambda'}^{i,i'} c_{\mathbf{k},\Lambda'}^{i'}, \quad (1.61)$$

where we have introduced the $\{\Lambda, i\}$ representation of the T -matrix

$$T_{\Lambda\Lambda'}^{i,i'} = \sum_{\Lambda''} \Delta_{\Lambda\Lambda''}^i \left(\delta_{ii'} \delta_{\Lambda''\Lambda'} + \sum_{\Lambda'''} G_{\Lambda''\Lambda'''}^{\text{imp},ii'} \Delta t_{\Lambda'''\Lambda'}^{\text{imp},i'} \right). \quad (1.62)$$

Chapter 2

Impurity-driven spin-orbit torques

2.1 Spin-orbit torques

The spin-orbit torque (SOT) can be described as a precession of magnetization in response to an electric current. This precession is mediated through the spin-orbit coupling in the studied system, which converts the orbital angular momentum of the conduction electrons to spin angular momentum of magnetic atoms.

The discussion of spin-orbit torques is related to the problem of the description of the magnetization dynamics. The equation of motion for the magnetization $\hat{\mathbf{M}}$ in the presence of spin-orbit torque is given by the Landau-Lifshitz-Gilbert (LLG) equation in addition to the spin-orbit torque term

$$\frac{d\hat{\mathbf{M}}}{dt} = -|\gamma|\hat{\mathbf{M}} \times \mathbf{S}^{eff} + \alpha\hat{\mathbf{M}} \times \frac{d\hat{\mathbf{M}}}{dt} - \frac{|\gamma|}{\mu_0 M \Omega} \mathbf{T}(\mathbf{E}), \quad (2.1)$$

where $\hat{\mathbf{M}}$ is the direction and M is the magnitude of the magnetization. The factor $|\gamma|$ is the gyromagnetic ratio of electrons and α is the Gilbert damping. The precession of the magnetization around the effective field \mathbf{S}^{eff} is described by the first term on the right-hand side of Eq. (2.1). The second term represents the fact that the magnetization tends to align with the effective field. The last term, the so-called spin-orbit torque term, describes the change on the magnetization due to current-induced spin-orbit torque $\mathbf{T}(\mathbf{E})$.

In this thesis we study the linear response of the spin-orbit torque to an applied electric field \mathcal{E} , which is represented by the torkance tensor \mathbf{t} ,

$$\mathbf{T}(\mathbf{E}) = \mathbf{t}\mathcal{E} \quad (2.2)$$

If we observe how the SOT, the electric field and the torkance are transformed under the inversion operator \mathcal{I} , we will find that the torkance vanishes in a system which is characterized by inversion symmetry [20]. Therefore, a finite response of the torque to the electric field, i.e. a non zero torkance tensor, exists only in the case of a non-centrosymmetric system. In this work, the topological insulators surface is studied, i.e. no inversion symmetry exists.

2.1.1 Kubo formalism

According to the Kubo linear response formalism the torkance tensor \mathbf{t} , as defined by Eq. (2.2), has the following three contributions [21]¹

$$t_{ij}^{\text{I(a)}} = \frac{e}{\hbar} \int_{-\infty}^{\infty} dE \frac{df(E)}{dE} \text{Tr} \langle \mathcal{T}_i G^R(E) v_j G^A(E) \rangle \quad (2.3)$$

$$t_{ij}^{\text{I(b)}} = -\frac{e}{\hbar} \int_{-\infty}^{\infty} dE \frac{df(E)}{dE} \text{ReTr} \langle \mathcal{T}_i G^R(E) v_j G^R(E) \rangle \quad (2.4)$$

$$t_{ij}^{\text{II}} = -\frac{e}{\hbar} \int_{-\infty}^{\infty} dE f(E) \text{ReTr} \left\langle \mathcal{T}_i G^R(E) v_j \frac{dG^R(E)}{dE} - \mathcal{T}_i \frac{dG^R(E)}{dE} v_j G^R(E) \right\rangle, \quad (2.5)$$

where \hbar is the Planck's constant, $f(E)$ is the Fermi-Dirac distribution function, v_j is the j th component of the velocity operator and \mathcal{T}_i is the i th Cartesian component of the torque operator. On the above equations $G^R(E)$ and $G^A(E)$ represent the retarded and advanced Green functions, respectively. The first two contributions (Eq. (2.3),(2.4)) are referred as Fermi surface terms. Their calculation implies the knowledge of the Green function at the Fermi energy only, as the derivative of the distribution function $\frac{df(E)}{dE}$ reduces to a Dirac distribution in the limit of low temperatures ($T \rightarrow 0$). The third contribution (Eq. (2.5)) is called Fermi sea contribution, as it depends on an integral over all occupied states.

The torque operator is defined as

$$\mathcal{T}(\mathbf{r}) = -\mu_B \boldsymbol{\sigma} \times \mathbf{B}^{\text{xc}}(\mathbf{r}), \quad (2.6)$$

where $\boldsymbol{\sigma}$ is the vector of Pauli spin matrices and $\mathbf{B}^{\text{xc}}(\mathbf{r})$ is the exchange field. The determination of the exchange field requires the use of *ab initio* calculations, as it varies rapidly at the atomic scale.

The retarded and advanced Green functions in Eq. (2.3)-(2.5), are defined as $G^R(E) = \hbar[E - H + i\Gamma]^{-1}$ and $G^A(E) = \hbar[E - H - i\Gamma]^{-1}$, where $\Gamma(E)$ is the self energy due to the disorder or electron-phonon scattering in the system. Using the constant effective band broadening Γ , which is equivalent to a constant relaxation time approximation, we can be inserted in our investigation the influence of disorder in the system.

The torkance tensor \mathbf{t} is decomposed into even and odd components as $t_{ij} = t_{ij}^{\text{even}} + t_{ij}^{\text{odd}}$, with respect to the direction of magnetization $\hat{\mathbf{M}}$. In this work we will investigate only the odd components of the torkance, since they are dependent on the scattering mechanisms which present in the system. Considering the limit $\Gamma \rightarrow 0$, the so-called clean limit, the odd component of the torkance tensor takes the form [22]

$$t_{ij}^{\text{odd}} = \frac{e\hbar}{2\Gamma\mathcal{N}} \sum_{\mathbf{k}n} \langle \psi_{\mathbf{k}n} | \mathcal{T}_i | \psi_{\mathbf{k}n} \rangle \langle \psi_{\mathbf{k}n} | v_j | \psi_{\mathbf{k}n} \rangle \frac{\partial f(E_{\mathbf{k}n})}{\partial E}, \quad (2.7)$$

with \hbar the reduced Planck's constant, \mathbf{k} the Bloch vector and \mathcal{N} the number of the \mathbf{k} -points in the Brillouin zone. With $\psi_{\mathbf{k}n}$ and $E_{\mathbf{k}n}$ are symbolized the eigenfunctions and

¹We set $e = -|e|$, the electron's charge.

eigenenergies of the system, respectively, with n a band index. From Eq. (2.7) it follows that the odd part of the torque diverges as $1/\Gamma$, i.e. it is proportional to the quasi-particle lifetime. In Section (2.3) we will treat the odd torque based in Boltzmann formalism in the low-temperature limit.

2.2 KKR Representation of Operators

The calculation of the torque which is exerted at an impurity atom implies a calculation of the torque expectation values of individual electronic states. In this Section, following G. Geranton [20] analysis, we present the expressions for expectation values of the spin and the torque operators based on the KKR formalism. We can also determine to what extent the torque arises from spin currents, computing the expectation value of the spin flux operator.

2.2.1 Spin expectation value

The contribution of a state \mathbf{k} to the i -th component of the spin at the atom μ is given as the expectation value of the spin operator $\boldsymbol{\sigma}$:

$$\langle \sigma_{i\mu} \rangle_{\mathbf{k}} = \left\langle \psi_{\mathbf{k}}^{\text{imp}} \left| \sigma_{i\mu} \right| \psi_{\mathbf{k}}^{\text{imp}} \right\rangle = \int_{\Omega_{\mu}} d\mathbf{r} [\psi_{\mathbf{k}}^{\text{imp}}(\mathbf{r})]^{\dagger} \sigma_i [\psi_{\mathbf{k}}^{\text{imp}}(\mathbf{r})] \quad (2.8)$$

The space integration can be extended to the entire space introducing the shape function $\theta(\mathbf{r})$ (Eq. (1.5)) of the atomic cells in the integral. Expanding the wavefunction of the impurity atom μ ($\psi_{\mathbf{k}}^{\text{imp},\mu}$) into the regular scattering solutions ($R_{\Lambda}^{\text{imp},\mu}$) according to Eq. (1.49) the spin expectation value is written

$$\langle \sigma_{i\mu} \rangle_{\mathbf{k}} = \sum_{\Lambda} \sum_{\Lambda'} [c_{\Lambda}^{\text{imp},\mu}]^* c_{\Lambda'}^{\text{imp},\mu} \int d\mathbf{r} \theta^{\mu}(\mathbf{r}) [R_{\Lambda}^{\text{imp},\mu}(\mathbf{r}; E)]^{\dagger} \sigma_i R_{\Lambda'}^{\text{imp},\mu}(\mathbf{r}; E) \quad (2.9)$$

Defining the spin matrix elements as [23]

$$\Sigma_{\Lambda\Lambda',i}^{\mu} = \int d\mathbf{r} \theta^{\mu}(\mathbf{r}) [R_{\Lambda}^{\text{imp},\mu}(\mathbf{r}; E)]^{\dagger} \sigma_i R_{\Lambda'}^{\text{imp},\mu}(\mathbf{r}; E), \quad (2.10)$$

Eq. (2.9) is written in the form of a matrix multiplication

$$\langle \sigma_{i\mu} \rangle_{\mathbf{k}} = \sum_{\Lambda} \sum_{\Lambda'} [c_{\Lambda}^{\text{imp},\mu}]^* \Sigma_{\Lambda\Lambda',i}^{\mu} c_{\Lambda'}^{\text{imp},\mu} \quad (2.11)$$

Since both the shape function $\theta^{\mu}(\mathbf{r})$ and the scattering solutions $R_{\Lambda}^{\text{imp},\mu}(\mathbf{r}; E)$ are expanded in real spherical harmonics, according to Equations (1.7) and (1.51) respectively, the spin matrix elements are finally written as

$$\Sigma_{LL',i}^{ss',\mu} = \sum_{L_1 L_2 L_3} C_{L_1 L_2 L_3} \int dr \theta_{L_1}^{\mu}(r) [R_{L_2 L}^{\text{imp},s,\mu}(r)]^{\dagger} \sigma_i R_{L_3 L'}^{\text{imp},s',\mu}(r) \quad (2.12)$$

2.2.2 Torque expectation value

According to the definition of the torque operator (Eq. 2.6) its components are given by the equation

$$\mathcal{T}_i(\mathbf{r}) = -\mu_B \sum_{jk} \epsilon_{ijk} \sigma_j B_k(\mathbf{r}), \quad (2.13)$$

where ϵ_{ijk} is the Levi-Civita symbol and the indices i, j, k take the values x, y and z .

The expectation value of the torque exerted on a state \mathbf{k} of the atom μ due to an external electric field is calculated, using Eq. (2.13), by the following relation

$$\langle \mathcal{T}_{i\mu} \rangle_{\mathbf{k}} = \langle \psi_{\mathbf{k}}^{\text{imp}} | \mathcal{T}_{i\mu} | \psi_{\mathbf{k}}^{\text{imp}} \rangle \quad (2.14)$$

$$= -\mu_B \sum_{jk} \epsilon_{ijk} \int_{\Omega_\mu} d\mathbf{r} [\psi_{\mathbf{k}}^{\text{imp}}(\mathbf{r})]^\dagger \sigma_j [\psi_{\mathbf{k}}^{\text{imp}}(\mathbf{r})] B_k(\mathbf{r}) \quad (2.15)$$

With respect to Eq. (2.9), the previous equation takes the form

$$\langle \mathcal{T}_{i\mu} \rangle_{\mathbf{k}} = \sum_{\Lambda} \sum_{\Lambda'} [c_{\Lambda}^{\text{imp},\mu}]^* \mathfrak{T}_{\Lambda\Lambda',i}^{\mu} c_{\Lambda'}^{\text{imp},\mu}, \quad (2.16)$$

where the matrix elements $\mathfrak{T}_{\Lambda\Lambda',i}^{\mu}$ are defined by the following equation

$$\mathfrak{T}_{\Lambda\Lambda',i}^{\mu} = -\mu_B \sum_{jk} \epsilon_{ijk} \int d\mathbf{r} \theta^\mu(\mathbf{r}) [R_{\Lambda}^{\text{imp},\mu}(\mathbf{r}; E)]^\dagger \sigma_j R_{\Lambda'}^{\text{imp},\mu}(\mathbf{r}; E) B_k^\mu(\mathbf{r}) \quad (2.17)$$

In the above equation (2.17) space integration extended to the entire space using the shape function $\theta^\mu(\mathbf{r})$ of the atomic cell.

The scattering solutions $R_{\Lambda}^{\text{imp},\mu}(\mathbf{r})$, the shape function $\theta_\mu(\mathbf{r})$ and the exchange field $B_k^\mu(\mathbf{r})$ are expanded in spherical harmonics. Defining the convoluted exchange field as $b_k^\mu(\mathbf{r}) = B_k^\mu(\mathbf{r})\theta_\mu(\mathbf{r})$ the calculation of the two spherical harmonics of the exchange field and the shape function is restricted to one for the convoluted exchange field $b_k^\mu(\mathbf{r})$:

$$b_k^\mu(\mathbf{r}) = \sum_{L_3} b_{L_3,k}^\mu Y_{L_3}(\hat{r}) \quad (2.18)$$

Replacing that in Eq. (2.17) the torque matrix elements are finally calculated in the KKR formalism by the relation

$$\mathfrak{T}_{LL',i}^{ss',\mu} = -\mu_B \sum_{jk} \epsilon_{ijk} \sum_{L_1 L_2 L_3} C_{L_1 L_2 L_3} \int dr [R_{L_1 L}^{\text{imp},s,\mu}(r)]^\dagger \sigma_j R_{L_2 L'}^{\text{imp},s',\mu}(r) b_{L_3,k}^\mu(r) \quad (2.19)$$

2.2.3 Spin flux expectation value

The spin flux operator is equivalent to the spin current operator, but represents the magnetic moment through the spin current which enters to a sphere of muffin-tin radius, r_{MT}^2 , around an atom.

²The muffin-tin radius is equal to the half of the first neighbor distance.

The expectation value of the spin flux operator of a state at the atom μ is given according to the relation

$$\begin{aligned} \langle \mathcal{Q}_{i\mu} \rangle_{\mathbf{k}} &= \left\langle \psi_{\mathbf{k}}^{\text{imp}} \left| \mathcal{Q}_{i\mu} \right| \psi_{\mathbf{k}}^{\text{imp}} \right\rangle \\ &= \frac{\mu_B \hbar}{2ie} \int_{S_\mu} d\mathbf{S} \left[[\psi_{\mathbf{k}}^{\text{imp}}(\mathbf{r})]^\dagger \sigma_i \nabla \psi_{\mathbf{k}}^{\text{imp}}(\mathbf{r}) - [\nabla \psi_{\mathbf{k}}^{\text{imp}}(\mathbf{r})]^\dagger \sigma_i \psi_{\mathbf{k}}^{\text{imp}}(\mathbf{r}) \right], \end{aligned} \quad (2.20)$$

where the integration takes place into the surface S_μ , which corresponds to the muffin-tin sphere of the atom μ . The integral into the surface of the muffin-tin sphere can be replaced by an integral over the solid angle $d\Omega$ according to relation $d\mathbf{S} = r_{\text{MT}}^2 \mathbf{e}_\Omega d\Omega$, where r_{MT} is the radius of the muffin-tin sphere and \mathbf{e}_Ω is the unit vector with direction to the center of the sphere.

Replacing the impurity wavefunction of atom μ by Eq. (1.49) the spin flux expectation value is written as a matrix multiplication:

$$\langle \mathcal{Q}_{i\mu} \rangle_{\mathbf{k}} = \sum_{\Lambda} \sum_{\Lambda'} [c_{\Lambda}^{\text{imp},\mu}]^* q_{\Lambda\Lambda',i}^{\mu} c_{\Lambda'}^{\text{imp},\mu}, \quad (2.21)$$

where the matrix elements $q_{\Lambda\Lambda',i}^{\mu}$ are defined as

$$q_{\Lambda\Lambda',i}^{\mu} = \frac{\mu_B \hbar}{2ie} \int_{S_\mu} d\mathbf{S} \left[[R_{\Lambda}^{\text{imp},\mu}(\mathbf{r}; E)]^\dagger \sigma_i \nabla R_{\Lambda'}^{\text{imp},\mu}(\mathbf{r}; E) - [\nabla R_{\Lambda}^{\text{imp},\mu}(\mathbf{r}; E)]^\dagger \sigma_i R_{\Lambda'}^{\text{imp},\mu}(\mathbf{r}; E) \right] \quad (2.22)$$

Replacing the integral into the surface and expanding the regular solutions $R_{\Lambda}^{\text{imp},\mu}$ in spherical harmonics, the spin flux matrix elements in the KKR representation are given by

$$q_{LL',i}^{ss',\mu} = \frac{\mu_B \hbar}{2ie} \sum_{L_1} \left[[R_{L_1 L}^{\text{imp},s,\mu}(r)]^\dagger \sigma_i \frac{\partial}{\partial r} \left(R_{L_1 L'}^{\text{imp},s',\mu}(r) \right) - \frac{\partial}{\partial r} \left([R_{L_1 L}^{\text{imp},s,\mu}(r)]^\dagger \right) \sigma_i R_{L_1 L'}^{\text{imp},s',\mu}(r) \right]_{r=r_{\text{MT}}} \quad (2.23)$$

2.3 Boltzmann formalism for the spin-orbit torque

In this work we will investigate transport phenomena on Fermi surface. A very fruitful formalism to describe such phenomena is based on the semiclassical approach³. In this Section we present the calculation of the impurity-driven spin-orbit torque, of the spin and of the spin-accumulation, applying the Boltzmann formalism.

2.3.1 Boltzmann transport equation

Within the semiclassical approach, the crystal electrons are viewed as a wavepacket of Bloch states with a width Δk in reciprocal space, which spreads only over a distance $\Delta r \sim 1/\Delta k$, according to the Heisenberg uncertainty principle.

We can define the distribution function $f_{\mathbf{k}}(\mathbf{r}, t)$ of a non-equilibrium system, which gives the electrons concentration in a finite region on time t . This is written as sum of

³The Boltzmann equation was first combined with KKR theory by Mertig and co-workers [24].

two terms, of the Fermi-Dirac function $f^0(E_{\mathbf{k}})$ (equilibrium distribution function) and of the deviation by the equilibrium due to the external forces, $g_{\mathbf{k}}$,

$$f_{\mathbf{k}} = f^0(E_{\mathbf{k}}) + g_{\mathbf{k}} \quad (2.24)$$

The flow of the distribution function in the presence of external forces and as a result of electron scattering processes can be investigated by the Boltzmann equation:

$$\frac{\partial f_{\mathbf{k}}}{\partial t} + \frac{\partial f_{\mathbf{k}}}{\partial t} \Big|_{\text{field}} + \frac{\partial f_{\mathbf{k}}}{\partial t} \Big|_{\text{diffusion}} = \frac{\partial f_{\mathbf{k}}}{\partial t} \Big|_{\text{sc}} \quad (2.25)$$

For a homogeneous and time-independent external electric field and in the description of a steady state, i.e. $\frac{\partial f_{\mathbf{k}}}{\partial t} = 0$, only the field term on the left-hand side in Eq. (2.25) survives. Then, the Boltzmann equation is written:

$$\frac{\partial f_{\mathbf{k}}}{\partial t} \Big|_{\text{field}} = \frac{\partial f_{\mathbf{k}}}{\partial t} \Big|_{\text{sc}} \quad (2.26)$$

The motion of an electron wavepacket in an external electric field \mathcal{E} , is described by the semiclassical equations

$$\dot{\mathbf{r}} = \mathbf{v}_{\mathbf{k}} = \frac{1}{\hbar} \frac{\partial E_{\mathbf{k}}}{\partial \mathbf{k}} \quad (2.27)$$

$$\dot{\mathbf{k}} = \frac{e}{\hbar} \mathcal{E}, \quad (2.28)$$

where in Eq. (2.27) we defined the group velocity $\mathbf{v}_{\mathbf{k}}$. Making use of the chain rule for the derivative and using Eq. (2.28), the Boltzmann equation (2.26) reads

$$\begin{aligned} \frac{\partial f_{\mathbf{k}}}{\partial t} \Big|_{\text{field}} &= \frac{\partial f_{\mathbf{k}}}{\partial \mathbf{k}} \cdot \frac{d\mathbf{k}}{dt} \Rightarrow \\ \frac{\partial f_{\mathbf{k}}}{\partial t} \Big|_{\text{field}} &= \frac{e}{\hbar} \nabla_{\mathbf{k}} f_{\mathbf{k}} \cdot \mathcal{E} \end{aligned} \quad (2.29)$$

If we are only interested in phenomena that depend linearly on the external field we can replace $f_{\mathbf{k}}$ by $f^0(E_{\mathbf{k}})$ on the right hand side of Eq. (2.29), because the term $\nabla_{\mathbf{k}} g_{\mathbf{k}} \cdot \mathcal{E}$ is higher than first order term and can be dropped ⁴:

$$\frac{\partial f_{\mathbf{k}}}{\partial t} \Big|_{\text{field}} = \frac{e}{\hbar} \nabla_{\mathbf{k}} f^0(E_{\mathbf{k}}) \cdot \mathcal{E} \quad (2.30)$$

Inserting the group velocity of Bloch's electrons (2.27) in Eq. (2.30), we arrive at the following form for the field term [25]:

$$\frac{\partial f_{\mathbf{k}}}{\partial t} \Big|_{\text{field}} = e \frac{\partial f^0(E_{\mathbf{k}})}{\partial E_{\mathbf{k}}} \mathbf{v}_{\mathbf{k}} \cdot \mathcal{E} \quad (2.31)$$

The scattering term can be written in its most general form by using the quantum-mechanical transition rate $w_{\mathbf{k}\mathbf{k}'}$. The rate of change of the distribution $f_{\mathbf{k}}$ is built up

⁴In the low-temperature limit the deviation $g_{\mathbf{k}}$ will be linear in the electric field ($g_{\mathbf{k}} \propto \mathcal{E}$).

of two terms, one increasing the value of f for the electrons that are scattered from all other states \mathbf{k}' into the state \mathbf{k} and one reducing the value of f for the electrons that are scattered out from the state \mathbf{k} to all others [26].

$$\left. \frac{\partial f_{\mathbf{k}}}{\partial t} \right|_{\text{sc}} = \sum_{\mathbf{k}'} (f_{\mathbf{k}'} w_{\mathbf{k}\mathbf{k}'} - f_{\mathbf{k}} w_{\mathbf{k}'\mathbf{k}}) \quad (2.32)$$

$$= \sum_{\mathbf{k}'} (g_{\mathbf{k}'} w_{\mathbf{k}\mathbf{k}'} - g_{\mathbf{k}} w_{\mathbf{k}'\mathbf{k}}) + \sum_{\mathbf{k}'} (f^0(E_{\mathbf{k}'}) w_{\mathbf{k}\mathbf{k}'} - f^0(E_{\mathbf{k}}) w_{\mathbf{k}'\mathbf{k}}) \quad (2.33)$$

The following argument shows that only the first term of Eq. (2.33) survives. In the limit of vanishing electric field, i.e. in the equilibrium state, the rhs of Eq. (2.31) vanishes. Then, the Eq. (2.32) for the equilibrium state inserting the Fermi function reads $\sum_{\mathbf{k}'} (f^0(E_{\mathbf{k}'}) w_{\mathbf{k}\mathbf{k}'} - f^0(E_{\mathbf{k}}) w_{\mathbf{k}'\mathbf{k}}) = 0$.

It is significant to mention that in a crystalline solid the transition rate $w_{\mathbf{k}\mathbf{k}'}$, corresponding to a single defect, should be scaled by the number of defects in the crystal (assuming that all defects are of the same type), i.e. $w_{\mathbf{k}\mathbf{k}'} \rightarrow x_c N_{\text{cr}} w_{\mathbf{k}\mathbf{k}'}$, where x_c is the defect concentration and N_{cr} is the number of atoms in the crystal.

We can find the linearized expression with respect to the electric field for the distribution function due to defects, by introducing the mean free path $\Lambda_{\mathbf{k}}$:

$$g_{\mathbf{k}} = -e \frac{\partial f^0(E_{\mathbf{k}})}{\partial E_{\mathbf{k}}} \boldsymbol{\mathcal{E}} \cdot \Lambda_{\mathbf{k}} \quad (2.34)$$

The mean free path $\Lambda_{\mathbf{k}}$ declares the average distance traveled by an electron between scattering events. During this ‘‘collisionless flight’’, the electron gains energy $-e\boldsymbol{\mathcal{E}} \cdot (\mathbf{r} - \mathbf{r}_0)$, as a result of its acceleration by the electric field, moving from the position of scattering \mathbf{r}_0 to \mathbf{r} . Setting, on the average, $\Lambda_{\mathbf{k}} = \langle \mathbf{r} - \mathbf{r}_0 \rangle$, the term $-e\boldsymbol{\mathcal{E}} \cdot \Lambda_{\mathbf{k}}$ corresponds to the average energy gained due to the acceleration. In this sense, the band energy may be considered as a function of \mathbf{r} in the presence of the electric field, i.e., $E_{\mathbf{k}} \rightarrow E_{\mathbf{k}} - e\boldsymbol{\mathcal{E}} \cdot (\mathbf{r} - \mathbf{r}_0)$ and thus $\nabla_{\boldsymbol{\mathcal{E}}} E_{\mathbf{k}} = -e(\mathbf{r} - \mathbf{r}_0)$. Expanding the non-equilibrium distribution function $f_{\mathbf{k}}$

$$f_{\mathbf{k}} = f^0(E_{\mathbf{k}}) + \boldsymbol{\mathcal{E}} \cdot \nabla_{\boldsymbol{\mathcal{E}}} f_{\mathbf{k}} + \dots, \quad (2.35)$$

and setting

$$\boldsymbol{\mathcal{E}} \cdot \nabla_{\boldsymbol{\mathcal{E}}} f_{\mathbf{k}} = \frac{\partial f_{\mathbf{k}}}{\partial E_{\mathbf{k}}} \boldsymbol{\mathcal{E}} \cdot \nabla_{\boldsymbol{\mathcal{E}}} E_{\mathbf{k}} \approx \frac{\partial f^0(E_{\mathbf{k}})}{\partial E_{\mathbf{k}}} \boldsymbol{\mathcal{E}} \cdot \nabla_{\boldsymbol{\mathcal{E}}} E_{\mathbf{k}}, \quad (2.36)$$

we obtain to another form of the deviation function, in terms of the derivative of the equilibrium distribution function:

$$\begin{aligned} g_{\mathbf{k}} = f_{\mathbf{k}} - f^0(E_{\mathbf{k}}) &= \frac{\partial f^0(E_{\mathbf{k}})}{\partial E_{\mathbf{k}}} \boldsymbol{\mathcal{E}} \cdot \nabla_{\boldsymbol{\mathcal{E}}} E_{\mathbf{k}} \\ &= -e \frac{\partial f^0(E_{\mathbf{k}})}{\partial E_{\mathbf{k}}} \boldsymbol{\mathcal{E}} \cdot (\mathbf{r} - \mathbf{r}_0), \end{aligned} \quad (2.37)$$

which justifies the choice (2.34).

In our study, we focus on the limit of low-temperatures ($T \rightarrow 0$), in which the derivative of the distribution function is proportional to the δ -function ($-\frac{\partial f^0(E_{\mathbf{k}})}{\partial E_{\mathbf{k}}} \rightarrow \delta(E_{\mathbf{k}} - E_F)$), and the deviation $g_{\mathbf{k}}$, as it was defined by Eq. (2.34), has the following form:

$$g_{\mathbf{k}} = e \delta(E_{\mathbf{k}} - E_F) \boldsymbol{\mathcal{E}} \cdot \Lambda_{\mathbf{k}} \quad (2.38)$$

Inserting Eq. (2.38) into Eq. (2.33), and accounting for the number of defects $x_c N_{\text{cr}}$, we arrive at another expression of the Boltzmann equation

$$\left. \frac{\partial f_{\mathbf{k}}}{\partial t} \right|_{\text{sc}} = \sum_{\mathbf{k}'} (g_{\mathbf{k}'} x_c N_{\text{cr}} w_{\mathbf{k}\mathbf{k}'} - g_{\mathbf{k}} x_c N_{\text{cr}} w_{\mathbf{k}'\mathbf{k}}) \Rightarrow \quad (2.39)$$

$$\left. \frac{\partial f_{\mathbf{k}}}{\partial t} \right|_{\text{sc}} = -N_{\text{cr}} e \frac{\partial f^0(E_{\mathbf{k}})}{\partial E_{\mathbf{k}}} \boldsymbol{\mathcal{E}} \cdot \sum_{\mathbf{k}'} (x_c \boldsymbol{\Lambda}_{\mathbf{k}'} w_{\mathbf{k}\mathbf{k}'} - x_c \boldsymbol{\Lambda}_{\mathbf{k}} w_{\mathbf{k}'\mathbf{k}}) \quad (2.40)$$

Combining Eqs. (2.26), (2.31) and (2.40) we arrive at a self-consistent equation of the vector mean free path $\boldsymbol{\Lambda}_{\mathbf{k}}$

$$\begin{aligned} e \frac{\partial f^0(E_{\mathbf{k}})}{\partial E_{\mathbf{k}}} \mathbf{u}_{\mathbf{k}} \cdot \boldsymbol{\mathcal{E}} &= -N_{\text{cr}} e \frac{\partial f^0(E_{\mathbf{k}})}{\partial E_{\mathbf{k}}} \boldsymbol{\mathcal{E}} \cdot \sum_{\mathbf{k}'} (x_c \boldsymbol{\Lambda}_{\mathbf{k}'} w_{\mathbf{k}\mathbf{k}'} - x_c \boldsymbol{\Lambda}_{\mathbf{k}} w_{\mathbf{k}'\mathbf{k}}) \Rightarrow \\ (x_c \boldsymbol{\Lambda}_{\mathbf{k}} \cdot \hat{n}_{\boldsymbol{\mathcal{E}}}) N_{\text{cr}} &= \frac{1}{\sum_{\mathbf{k}'} w_{\mathbf{k}'\mathbf{k}}} \left[\mathbf{v}_{\mathbf{k}} \cdot \hat{n}_{\boldsymbol{\mathcal{E}}} + N_{\text{cr}} \sum_{\mathbf{k}'} w_{\mathbf{k}\mathbf{k}'} (x_c \boldsymbol{\Lambda}_{\mathbf{k}'} \cdot \hat{n}_{\boldsymbol{\mathcal{E}}}) \right] \end{aligned} \quad (2.41)$$

It is worth noticing that the Eq. (2.41) depends only on the direction of the electric field, $\hat{n}_{\boldsymbol{\mathcal{E}}} = \boldsymbol{\mathcal{E}}/|\boldsymbol{\mathcal{E}}|$, which is expected since we are only seeking the linear response of the system to the electric field. Thus, we obtain two independent equations, one for each component of the vector $\boldsymbol{\Lambda}_{\mathbf{k}}$. We can further manipulate Eq. (2.41) by defining the relaxation time $\tau_{\mathbf{k}} = 1/\sum_{\mathbf{k}'} w_{\mathbf{k}'\mathbf{k}}$.

$$(x_c \boldsymbol{\Lambda}_{\mathbf{k}} \cdot \hat{n}_{\boldsymbol{\mathcal{E}}}) N_{\text{cr}} = \tau_{\mathbf{k}} \left[\mathbf{v}_{\mathbf{k}} \cdot \hat{n}_{\boldsymbol{\mathcal{E}}} + N_{\text{cr}} \sum_{\mathbf{k}'} w_{\mathbf{k}\mathbf{k}'} (x_c \boldsymbol{\Lambda}_{\mathbf{k}'} \cdot \hat{n}_{\boldsymbol{\mathcal{E}}}) \right] \quad (2.42)$$

The above Eq. (2.42) is solved iteratively, according to the flow diagram which is presented in Appendix 4.

According to the Pauli principle, electrons which are far from Fermi level cannot make transitions to nearby states increasing their energy, since all neighboring higher energy states are occupied. Only the electrons at the Fermi surface are capable of absorbing energy in infinitesimal quantities. Therefore, the transports phenomena are related with the behavior of electrons at Fermi surface.

In view of the need to chart the Fermi surface, we introduce a local coordinate $(k'_{\perp}, k'_{\parallel})$ on the surface. Thus, the crystal momentum element is decomposed $d^2 \mathbf{k}' = dk'_{\perp} dk'_{\parallel}$, where k'_{\perp} is the component of \mathbf{k}' perpendicular to the surface, i.e. in the direction of the velocity, and k'_{\parallel} is oriented in the surface. Then, the summation over the index \mathbf{k}' , making use of the chain rule, becomes an integration over the energies and the integration over the isoenergy line

$$\sum_{\mathbf{k}'} \longrightarrow \frac{1}{S_{\text{rec}}} \int_{\text{BZ}} d^2 \mathbf{k}' = \frac{1}{S_{\text{rec}}} \int dE \int_{E_{\mathbf{k}}=E_{\text{F}}} \frac{dk'_{\parallel}}{\hbar |\mathbf{v}_{\mathbf{k}'}|} \quad (2.43)$$

where $S_{\text{rec}} = S_{\text{BZ}}/N_{\text{cr}} = (2\pi)^2/S_{\text{cr}}$ is the surface element of the reciprocal lattice, S_{BZ} is the Brillouin zone surface and S_{cr} is the crystal surface area.

In the low-field limit the scattering is dominated by elastic scattering off impurities and the scattering rate is proportional to the Dirac δ -function, i.e. $w_{\mathbf{k}\mathbf{k}'} = \tilde{w}_{\mathbf{k}\mathbf{k}'} \delta(E_{\mathbf{k}} - E_{\mathbf{k}'})$.

Consequently, we obtain an integro-differential equation for the calculation of the vector mean free path $\Lambda_{\mathbf{k}}$, which is solved iteratively:

$$(x_c \Lambda_{\mathbf{k}} \cdot \hat{n}_{\mathcal{E}}) N_{\text{cr}} = \tau_{\mathbf{k}} \left[\mathbf{v}_{\mathbf{k}} \cdot \hat{n}_{\mathcal{E}} + \frac{N_{\text{cr}}}{S_{\text{rec}}} \int_{E_{\mathbf{k}}=E_{\text{F}}} \frac{dk'}{\hbar |\mathbf{v}_{\mathbf{k}'}|} w_{\mathbf{k}\mathbf{k}'} (x_c \Lambda_{\mathbf{k}'} \cdot \hat{n}_{\mathcal{E}}) \right] \quad (2.44)$$

The response of electrons under the application of an external electric field \mathcal{E} is described by Ohm law:

$$\mathbf{j} = \overleftarrow{\sigma} \mathcal{E} \quad (2.45)$$

Once the mean free path has been found (Eq. 2.44), the current density can be calculated by means of the distribution function:

$$\begin{aligned} \mathbf{j} &= \frac{e}{S_{\text{cr}}} \sum_{\mathbf{k}} \mathbf{v}_{\mathbf{k}} f_{\mathbf{k}} \\ &= \frac{e}{S_{\text{cr}} S_{\text{rec}}} \int \delta(E_{\mathbf{k}} - E_{\text{F}}) dE \int_{E_{\mathbf{k}}=E_{\text{F}}} \frac{dk_{\parallel}}{\hbar |\mathbf{v}_{\mathbf{k}}|} \mathbf{v}_{\mathbf{k}} g_{\mathbf{k}} \\ &= \frac{1}{x_c} \frac{e^2}{4\pi^2} \int_{E_{\mathbf{k}}=E_{\text{F}}} \frac{dk_{\parallel}}{\hbar |\mathbf{v}_{\mathbf{k}}|} \mathbf{v}_{\mathbf{k}} (x_c \Lambda_{\mathbf{k}} \cdot \mathcal{E}) \end{aligned} \quad (2.46)$$

Then, according to Eqs. (2.45), (2.46) we can obtain the conductivity tensor:

$$\sigma_{ij} = \frac{1}{x_c} \frac{e^2}{4\pi^2} \int_{E_{\mathbf{k}}=E_{\text{F}}} \frac{dk}{\hbar |\mathbf{v}_{\mathbf{k}}|} (\mathbf{v}_{\mathbf{k}})_i (x_c \Lambda_{\mathbf{k}})_j \quad (2.47)$$

2.3.2 Response tensors in Boltzmann formalism

The torque which is exerted on atom μ by the electric field is written in the Boltzmann formalism as

$$\begin{aligned} \mathbf{T}_{\mu} &= \sum_{\mathbf{k}} f_{\mathbf{k}} \langle \mathcal{T}_{\mu} \rangle_{\mathbf{k}} \\ &= \sum_{\mathbf{k}} (f_{\mathbf{k}}^0 + g_{\mathbf{k}}) \langle \mathcal{T}_{\mu} \rangle_{\mathbf{k}} \end{aligned} \quad (2.48)$$

Supposing that there is no torque in the equilibrium, only the second term of Eq. (2.48) survives. Then, the torque which depends on the deviation function reads

$$\mathbf{T}_{\mu} = \sum_{\mathbf{k}} g_{\mathbf{k}} \langle \mathcal{T}_{\mu} \rangle_{\mathbf{k}}, \quad (2.49)$$

where the torque expectation value is calculated by the Eq. (2.16).

Replacing the distribution function (2.34) in the above equation (2.49), the expression for the torque is written as an integral over the Fermi surface:

$$\mathbf{T}_{\mu} = -\frac{e}{S_{\text{BZ}}} \int d^2 \mathbf{k} \left(-\frac{\partial f^0(E_{\mathbf{k}})}{\partial E_{\mathbf{k}}} \right) (\Lambda_{\mathbf{k}} \cdot \mathcal{E}) \langle \mathcal{T}_{\mu} \rangle_{\mathbf{k}} \quad (2.50)$$

$$= -\frac{e}{\hbar S_{\text{BZ}}} \int_{E_{\mathbf{k}}=E_{\text{F}}} \frac{dk_{\parallel}}{|\mathbf{v}_{\mathbf{k}}|} (\Lambda_{\mathbf{k}} \cdot \mathcal{E}) \langle \mathcal{T}_{\mu} \rangle_{\mathbf{k}}. \quad (2.51)$$

The SOT is related to the electric field $\boldsymbol{\mathcal{E}}$ by the response tensor for the torque \mathbf{t}_μ , according to the relation [21]:

$$\mathbf{T}_\mu = \mathbf{t}_\mu \boldsymbol{\mathcal{E}} \quad (2.52)$$

It is easily proved that the torkance \mathbf{t}_μ is given by the equation:

$$\mathbf{t}_\mu = -\frac{e}{\hbar S_{\text{BZ}}} \int_{E_{\mathbf{k}}=E_{\text{F}}} \frac{dk_{\parallel}}{|\mathbf{v}_{\mathbf{k}}|} \langle \mathcal{T}_\mu \rangle_{\mathbf{k}} \otimes \boldsymbol{\Lambda}_{\mathbf{k}} \quad (2.53)$$

A similar Fermi surface integral to Eq. (2.51), can be calculated for the spin accumulation which is induced by the electric field on atom μ :

$$\mathbf{s}_\mu = -\frac{e\mu_B}{\hbar S_{\text{BZ}}} \int_{E_{\mathbf{k}}=E_{\text{F}}} \frac{dk_{\parallel}}{|\mathbf{v}_{\mathbf{k}}|} (\langle \boldsymbol{\sigma}_\mu \rangle_{\mathbf{k}} \otimes \boldsymbol{\Lambda}_{\mathbf{k}}) \cdot \boldsymbol{\mathcal{E}} \quad (2.54)$$

The response tensor for the spin accumulation, $\boldsymbol{\chi}_\mu$, is defined according to relation

$$\mathbf{s}_\mu = \boldsymbol{\chi}_\mu \boldsymbol{\mathcal{E}} \quad (2.55)$$

and finally is given by the equation:

$$\boldsymbol{\chi}_\mu = -\frac{e\mu_B}{\hbar S_{\text{BZ}}} \int_{E_{\mathbf{k}}=E_{\text{F}}} \frac{dk_{\parallel}}{|\mathbf{v}_{\mathbf{k}}|} \langle \boldsymbol{\sigma}_\mu \rangle_{\mathbf{k}} \otimes \boldsymbol{\Lambda}_{\mathbf{k}} \quad (2.56)$$

In a similar way, one can find the spin flux which is absorbed by the atom μ :

$$\boldsymbol{\mathcal{Q}}_\mu = \frac{e}{\hbar S_{\text{BZ}}} \int_{E_{\mathbf{k}}=E_{\text{F}}} \frac{dk_{\parallel}}{|\mathbf{v}_{\mathbf{k}}|} (\langle \boldsymbol{\mathcal{Q}}_\mu \rangle_{\mathbf{k}} \otimes \boldsymbol{\Lambda}_{\mathbf{k}}) \cdot \boldsymbol{\mathcal{E}} \quad (2.57)$$

Then, the response tensor for the spin flux, \mathbf{q}_μ , which is defined by the relation

$$\boldsymbol{\mathcal{Q}}_\mu = \mathbf{q}_\mu \boldsymbol{\mathcal{E}}, \quad (2.58)$$

yields the following expression of the Fermi surface integral:

$$\mathbf{q}_\mu = \frac{e}{\hbar S_{\text{BZ}}} \int_{E_{\mathbf{k}}=E_{\text{F}}} \frac{dk_{\parallel}}{|\mathbf{v}_{\mathbf{k}}|} \langle \boldsymbol{\mathcal{Q}}_\mu \rangle_{\mathbf{k}} \otimes \boldsymbol{\Lambda}_{\mathbf{k}} \quad (2.59)$$

According to above equations the response functions of each atom on system can be investigated. It is also significant to refer to the total torque of all magnetic atoms of system, which is defined as a sum over all atoms

$$\mathbf{T} = \sum_{\mu} \mathbf{T}_\mu \quad (2.60)$$

The total torkance tensor, which defined by Eq. (2.2), is written in Boltzmann formalism as

$$\mathbf{t} = -\frac{e}{\hbar S_{\text{BZ}}} \int_{E_{\mathbf{k}}=E_{\text{F}}} \frac{dk_{\parallel}}{|\mathbf{v}_{\mathbf{k}}|} \langle \mathcal{T} \rangle_{\mathbf{k}} \otimes \boldsymbol{\Lambda}_{\mathbf{k}}, \quad (2.61)$$

where $\mathcal{T} = \sum_{\mu} \mathcal{T}_\mu$ is the total torque operator.

Chapter 3

Spin-orbit torque in magnetically doped topological insulator surfaces

3.1 Introduction to topological insulators

Topology is a branch of mathematics concerned with certain geometrical properties of objects. Geometrical shapes which cannot be deformed into one another continuously are called topologically inequivalent. A simple example of such objects is a sphere and a torus (e.g. a doughnut). The sphere, as a closed surface, can be transformed into the shape of a torus only after making a hole on it. These two shapes are distinguished by an integer topological invariant called the genus, g , which is essentially the number of holes [27].

In analogy, the mathematically defined space, where topological objects are defined in Solid State Physics, is the space of crystal momentum \mathbf{k} of Bloch electrons. The existence or absence of holes of the above example, corresponds in appearance or absence of band inversion in band structure of the materials ¹.

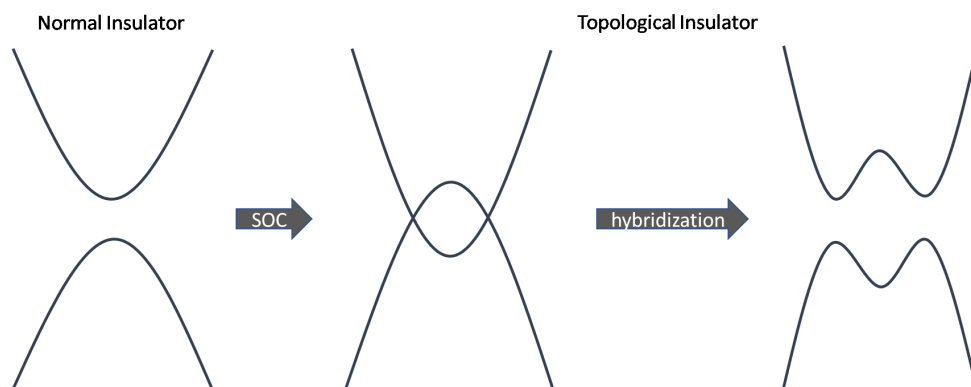


Figure 3.1: Schematic representation of the band inversion in band structures of the topological insulator.

¹In this thesis, the characteristics of topological insulators are given in summary. One can find more details on Refs. [15,28]

A normal insulator is characterized by an energy gap between the valence and the conduction band. In a topological insulator, the two bands are shifted across each other, closing the gap, due to strong spin-orbit coupling. Hybridization between the shifted bands leads to a reopening of the band gap, i.e. to a band inversion in band structures, as it is shown in Fig. (3.1).

In this thesis we focus on surfaces of the topological insulators due to its conduction surface states. The surface electronic states of a topological insulator are metallic-like states. The existence and the properties of these surface states are topologically protected, i.e. they are not destroyed by the perturbing surface potential (surface reconstruction). This property follows in a concrete mathematical sense that is derived from the symmetry and ordering of the bands in the bulk [1].

In addition, these states preserve the time-reversal symmetry of the system. On topological insulators surfaces the electrons with spin \mathbf{s} propagate only in one direction with crystal momentum \mathbf{k} , while the electrons of the opposite spin $-\mathbf{s}$ propagate only in the opposite direction with crystal momentum $-\mathbf{k}$. This uni-directionality has as a consequence an absence of back-scattering (from \mathbf{k} to $-\mathbf{k}$) off non-magnetic defects.

In this work, we investigate a system of a topological insulator surface doped with magnetic defects. It is important to note that in the presence of magnetic transition metal ions, the time-reversal symmetry is broken, due to the internal magnetic field, allowing the back-scattering.

3.2 Studied system: Bi_2Te_3 with Mn defects

As a host system we choose the surface of the topological insulator bismuth telluride, Bi_2Te_3 [29], modeled by a thick film. This film consists of 6 quintuple layers of Bi_2Te_3 “sandwiched” by 9 vacuum layers on top and 9 vacuum layers in the bottom, i.e. 78 sites.

Each quintuple layer is constructed by 10 sites, three Te atoms, two Bi atoms and five empty spheres ², placed between the atomic layers of Te and Bi. The interaction between atoms in a quintuple layer comes from strong covalent attraction, while interactions between quintuple layers originate from weaker Van der Waals ones [31]. This slab size is chosen, since on the one hand, it is thick enough to ensure the robustness of surface states and, on the other hand, it is thin enough to be numerically manageable by *ab initio* calculations.

The electronic structure of this film was computed using the Jülich KKR code. At first, a self-consistent calculation of the host system was carried out. The Fermi level was found to be in the middle of the band gap, using the Lloyd’s formula [32], correcting the truncation error due to the finite angular momentum cutoff ($l_{\text{max}} = 3$). In Fig. 3.2 the bandstructure of host material Bi_2Te_3 is presented. As we can observe, around the Fermi level the states form the so-called Dirac cone, which is a characteristic of topological insulators.

²These empty spheres have no nuclear charge and thus can be considered as virtual atoms, which are used to improve the sphericity of the constructed Voronoi cells [30].

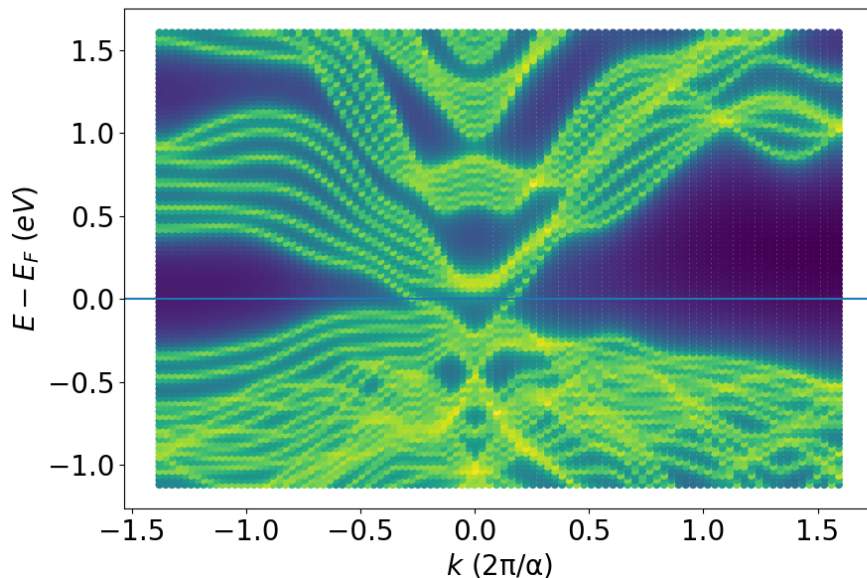


Figure 3.2: Band structure of Bi_2Te_3 thick film along $\text{M}\Gamma$ and ΓK directions. The Fermi level is $E_F = 8.6$ eV and the lattice constant is $\alpha = 19.79111$ Å.

The impurity system, which is studied in this work, is constructed by the Bi_2Te_3 surface doped with magnetic Mn atoms, embedded in interstitial positions. In particular, the impurity Mn atoms are placed in hollow site of the surface Te layer, following experiments on transition metals impurities on topological insulator surfaces [33,34], as it is shown in Fig. 3.3.

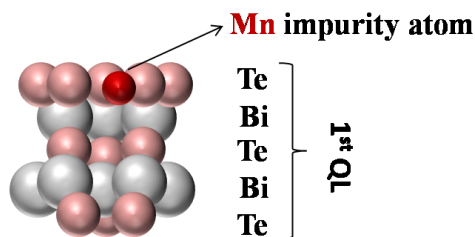


Figure 3.3: Illustration of the first quintuple layer of Bi_2Te_3 . The Mn impurity atom is embedded in interstitial position between the first layer of Te and the second layer of Bi.

In this work, two different approximations of the same system are studied. At first, we consider a single Mn impurity atom, which is embedded in the Bi_2Te_3 surface. Secondly, we study the case of 51 Mn impurity atoms on the surface of Bi_2Te_3 . The 51 Mn impurities occupy random positions in the two-dimensional surface lattice, within a disk of 1027 positions (Fig. 3.4), as it is shown in Fig. 3.4. This corresponds to a concentration of $\approx 5\%$ impurities. Choosing these two cases we can study the difference of Boltzmann equation with a single impurity scattering rate and with multiple scattering.

Considering a finite region with randomly distributed atoms on lattice sites, the central atom is the most representative, simulating a system with impurities, which are expanding to infinity. Therefore, we focus on the calculated quantities of the central atom.

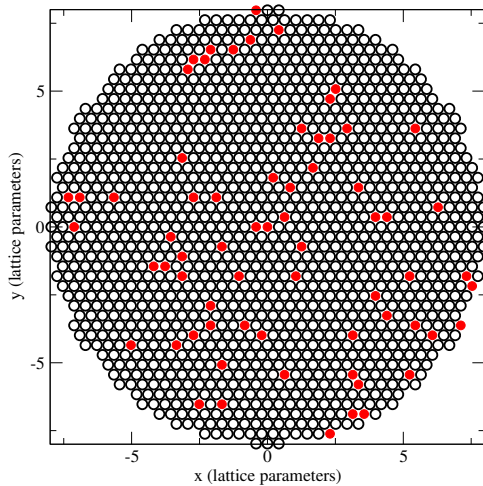


Figure 3.4: Illustration of the random positions of the impurities on the surface. Mn atoms are depicted in red.

The self-consistent potential of the defects was computed in a cluster of atoms, including the nearest neighbors of the defect, in order to account for the correct charge screening, with the Jülich KKR impurity-embedding code (KKRimp). At first, we calculate the potential of the single Mn impurity atom self-consistently, and then we approximate the potential in the case of 51 impurity atoms, replicating the potential of the isolated Mn impurity 51 times.

3.3 Scattering due to magnetic Mn defects

It is well known that the Fermi surface states are responsible for the spin transport properties in a metallic system. In topological insulators there are metallic surface states, therefore in our calculations we consider the states on the Fermi surface. A Jülich KKR code was used to map the Fermi surface of Bi_2Te_3 , solving the KKR secular equation (Eq. 1.33) [13]. The Fermi surface of the topological insulator Bi_2Te_3 film has the hexagonally warped form which is presented in Fig. 3.5.

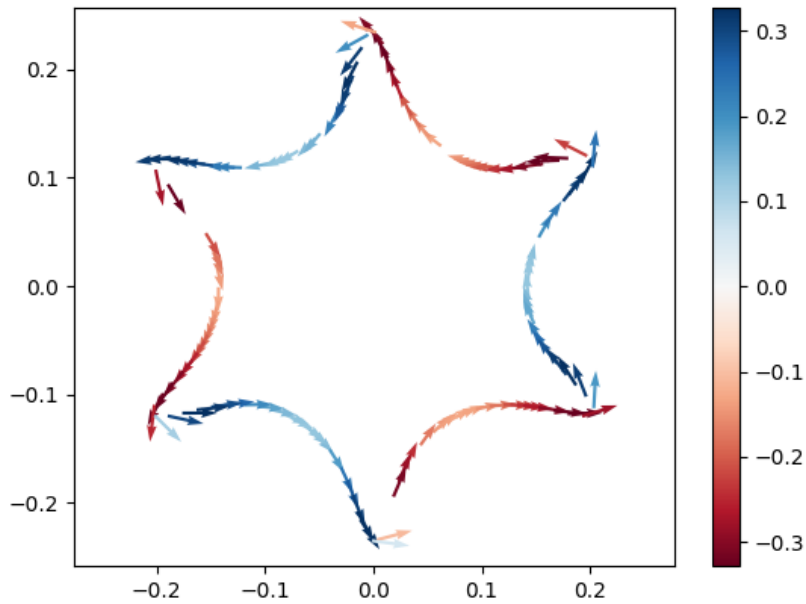


Figure 3.5: The spin-polarization of the surface states of Bi_2Te_3 film (top-view).

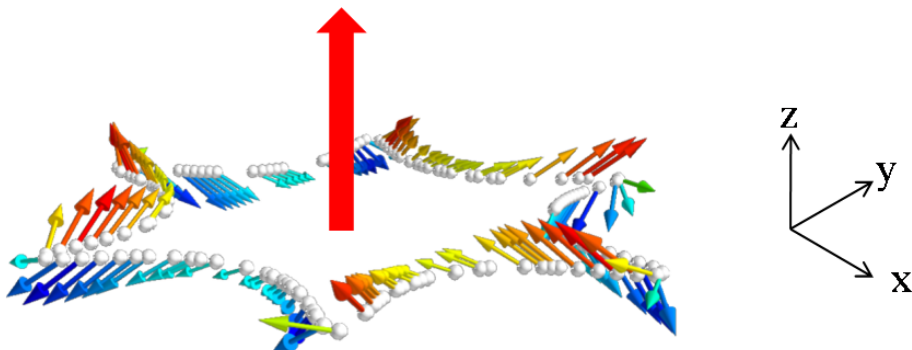


Figure 3.6: The spin-polarization of the surface states of Bi_2Te_3 film (side-view). The red arrow in the middle represents the magnetization of the Mn impurity. [Fig. adapted from Ref. [15]]

Fig. 3.5 represents the spin-polarization of states on Bi_2Te_3 surface. In Fig. 3.6 the spin-polarization of surface states of Bi_2Te_3 by a side-view, and the magnetization of the Mn impurity, are presented. As it is shown in Fig. 3.6, each state \mathbf{k} on the Fermi surface of Bi_2Te_3 is characterized by spin direction which is, to a large extent, parallel to the surface, while the magnetic moment of the impurity atom is perpendicular to the topological insulator surface, in agreement with experiments [34].

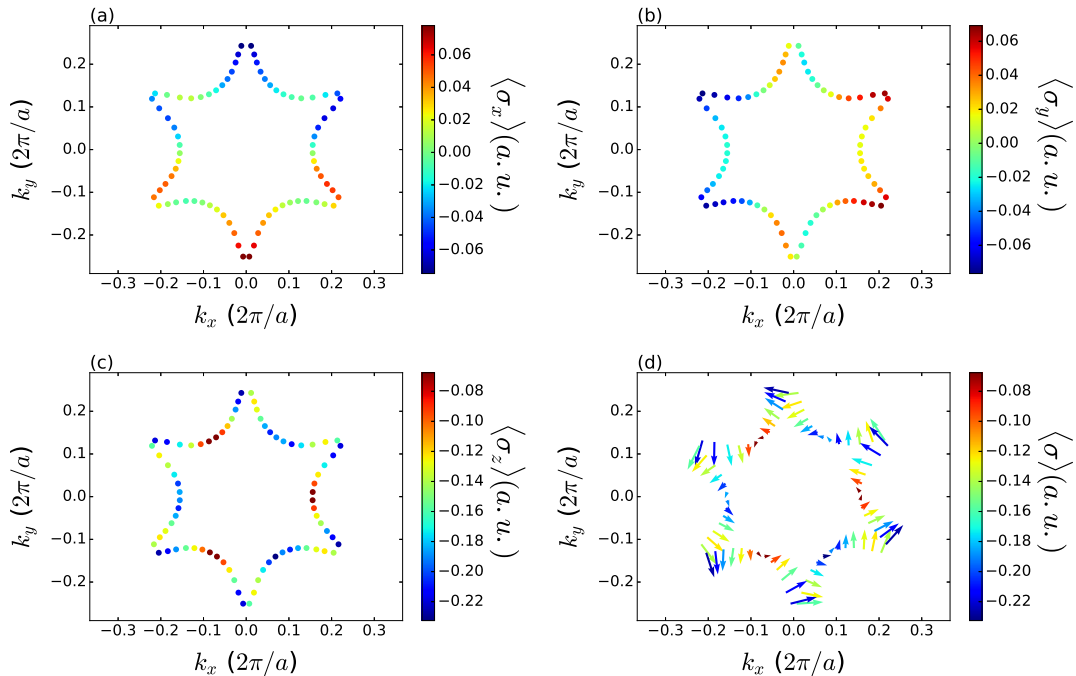


Figure 3.7: Expectation value of the x component of the spin $\langle \sigma_x \rangle$ (a), of the y component of the spin $\langle \sigma_y \rangle$ (b), and of the z component of the spin $\langle \sigma_z \rangle$ (c), for the scattering states on the Fermi surface integrated in the atomic cell of the Mn impurity, in the case of a single Mn impurity on the Bi_2Te_3 surface. (d) The same as in (a-c), but with the x and y components presented by arrows and the z component by a color code.

In the following, we first present the spin accumulation, torque, and spin flux in the impurity Mn atom, caused by each scattering state $\psi_{\mathbf{k}}^{\text{imp}}$ on the Fermi surface, separately. In a second step, these partial contributions are weighted and integrated, with the respective partial weights corresponding to the distribution function $g_{\mathbf{k}}$ and the mean free path $\Lambda_{\mathbf{k}}$, as it is self-consistently calculated by solving the Boltzmann equation (2.42).

According to Section 2.2.1 we compute the expectation value of the spin operator $\langle \sigma \rangle$ in the presence of one impurity atom in the host system. In Fig. 3.7(a-c) we show the expectation values of the components of the spin operator on the Fermi surface scattering states at the Mn atom, as they are computed according to Eq. (2.8). The spin projection on the $x - y$ plane is shown in Fig. 3.7(d). The spin polarization presents 120° rotation symmetry in the $x - y$ plane on the Fermi surface around the impurity axis (z axis), due to the crystal structure. In the symmetry considerations we note that, due to the magnetic field of the impurity, the time-reversal symmetry ($\mathbf{k} \rightarrow -\mathbf{k}$) as well as the reflection symmetry with respect to the $y - z$ plane are broken. Furthermore, we have to note that the magnetic moment of the Mn atom, corresponding to the Fermi surface, exists in z direction only. The integrated magnetic moment on $x - y$ plane vanishes, since the magnetic moment is in z direction of impurity atom.

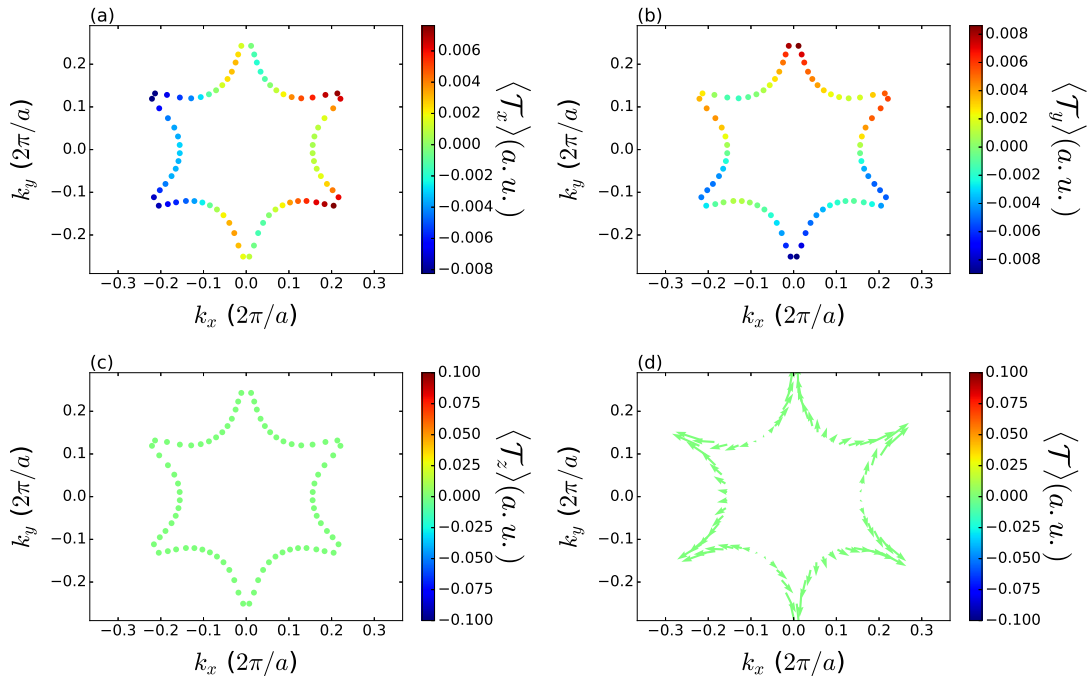


Figure 3.8: Expectation value of the x component of the torque $\langle \mathcal{T}_x \rangle$ (a), of the y component of the torque $\langle \mathcal{T}_y \rangle$ (b), and of the z component of the torque $\langle \mathcal{T}_z \rangle$ (c), for the scattering states on the Fermi surface integrated in the atomic cell of the Mn impurity, in the case of a single Mn impurity on the Bi_2Te_3 surface. (d) The same as in (a-c), but with the x and y components presented by arrows and the z component by a color code.

Next, we compute the expectation value of the torque exerted by each surface state on the impurity atom, based on Section 2.2.2. Each component of the torque expectation value, on the Fermi surface states on the impurity atom, as it is calculated by Eq. (2.14), is presented in Fig. 3.8(a-c). Obviously, there is no torque in the direction of the magnetization, as it is also proved by the external product which relates the torque with the magnetic field (Eq. 2.6). Therefore, the z component of the torque expectation value is zero, as it is shown in Fig. 3.8(c). We observe in Fig. 3.8(d) that the projection of the torque expectation value presents 120° rotation symmetry in the $x - y$ plane. Comparing Figs. 3.7 and 3.8, we find that the torque expectation value $\langle \mathcal{T}_y \rangle$ follows the opposite sign of the spin expectation value ($\langle -\sigma_x \rangle$), in accordance with Eq. (2.13). Also, the sign of the torque expectation value $\langle \mathcal{T}_x \rangle$ follows the sign of the spin expectation value ($\langle \sigma_y \rangle$), due to 90° rotation.

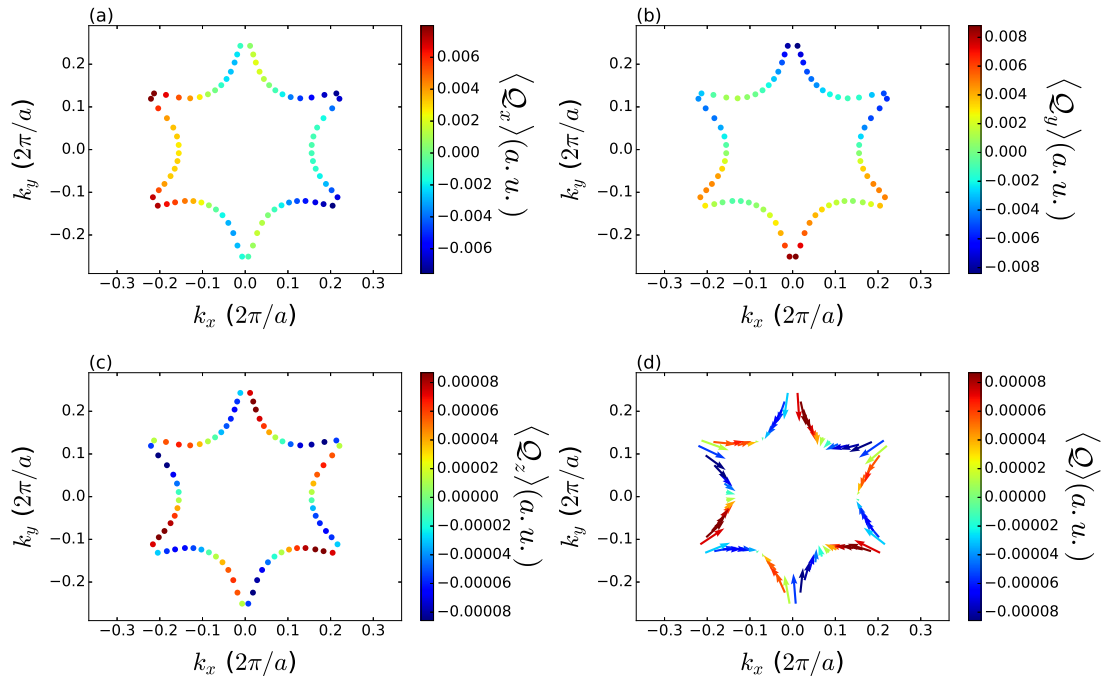


Figure 3.9: Expectation value of the x component of the spin flux $\langle \mathcal{Q}_x \rangle$ (a), of the y component of the spin flux $\langle \mathcal{Q}_y \rangle$ (b), and of the z component of the spin flux $\langle \mathcal{Q}_z \rangle$ (c), for the scattering states on the Fermi surface integrated in the atomic cell of the Mn impurity, in the case of a single Mn impurity on the Bi_2Te_3 surface. (d) The same as in (a-c), but with the x and y components presented by arrows and the z component by a color code.

As it was mentioned in Section 2.2.3 we can determine the part of the torque that arises from spin currents, by calculating the expectation value of the spin flux operator. Fig. 3.9(a-c) visualizes the expectation values of the components of the spin flux operator $\langle \mathcal{Q}_x \rangle$, $\langle \mathcal{Q}_y \rangle$, $\langle \mathcal{Q}_z \rangle$, which are calculated according to Eq. (2.20). In Fig. 3.9(d) the projection of the spin flux in the $x - y$ plane is presented. Comparing the Fig. 3.8 and Fig. 3.9 we observe that the expectation values of the spin flux operator $\langle -\mathcal{Q}_x \rangle$, $\langle -\mathcal{Q}_y \rangle$ are in agreement with the torque expectation values $\langle \mathcal{T}_x \rangle$, $\langle \mathcal{T}_y \rangle$, respectively. Therefore, we conclude that the torque on the impurity atom is mediated by the spin currents. As the previously measured quantities, the spin flux operator presents the symmetry of 120° rotation around the axis of the defect.

Next, the expectation values of the spin current, the torque and the spin flux will be studied for a larger number of magnetic impurities on the surface and they will be compared to the above results of the case of a single impurity on the surface. This way, we take into account the multiple scattering of the impurities.

We construct a system with 51 Mn atoms embedded in the surface of the host system. This corresponds to a concentration of $\approx 5\%$ impurities, as it was described to Section 3.2. We compute the expectation values of the spin, the spin-orbit torque and the spin flux for 10 different distributions of the impurities sites in the surface.

Since we want to model a random occupation by impurities in the infinitely large surface, we consider the central impurity atom in the disk as the most representative

for the average impurity in the physical system. In Figs 3.10, 3.11, 3.12 we present the calculated quantities for the representative central impurity atom, for one distribution selected out of ten. The calculations of the others distributions gave qualitatively similar results and they are omitted.

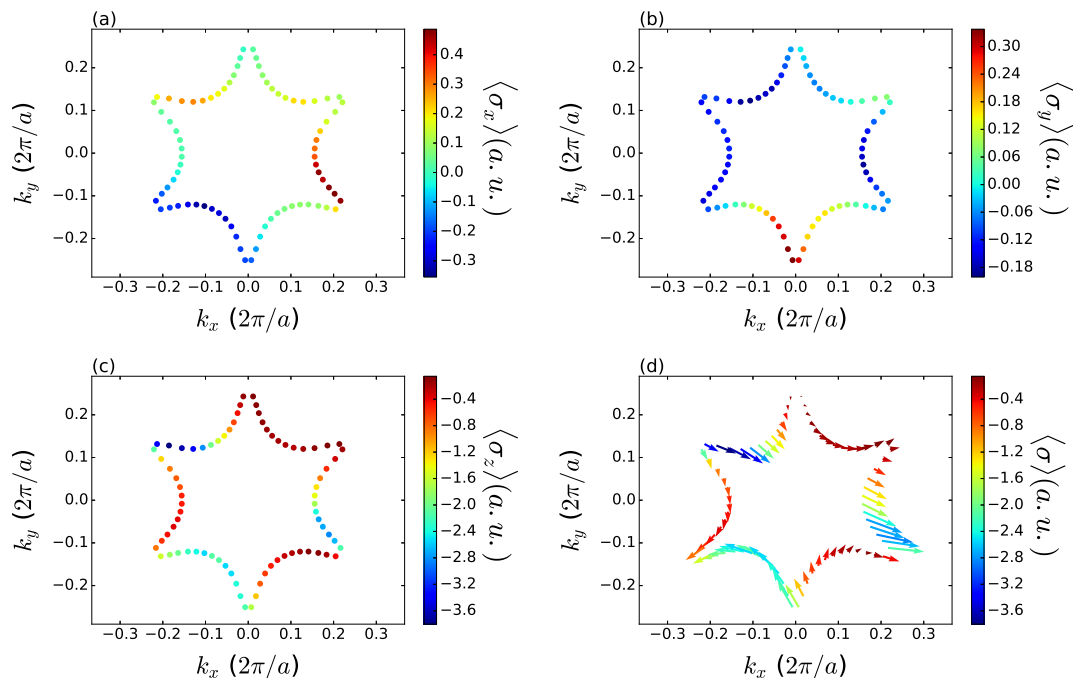


Figure 3.10: Expectation value of the x component of the spin $\langle \sigma_x \rangle$ (a), of the y component of the spin $\langle \sigma_y \rangle$ (b), and of the z component of the spin $\langle \sigma_z \rangle$ (c), for the scattering states on the Fermi surface integrated in the atomic cell of the central Mn impurity, in the case of 51 Mn impurities on the Bi_2Te_3 surface. (d) The same as in (a-c), but with the x and y components presented by arrows and the z component by a color code.

In Fig. 3.10(a-c), the components of the expectation values of the spin operator $\langle \sigma_x \rangle$, $\langle \sigma_y \rangle$, $\langle \sigma_z \rangle$ at the surface states of the central Mn atom are presented, as its projection in the $x - y$ plane, in the presence of 51 impurities on the surface.

Overall, we find a greater induced spin polarization at the surface states of the central impurity atom in the presence of many impurities on the surface, comparing Fig. 3.7 with 3.10. This enhancement of the spin values originates, obviously, from the multiple scattering of electrons. As it was expected, the 120° rotation symmetry in the $x - y$ plane on the Fermi surface is broken in the presence of 51 impurities into the crystal, as it is shown in Fig. 3.10(d), due to the change of the structure.

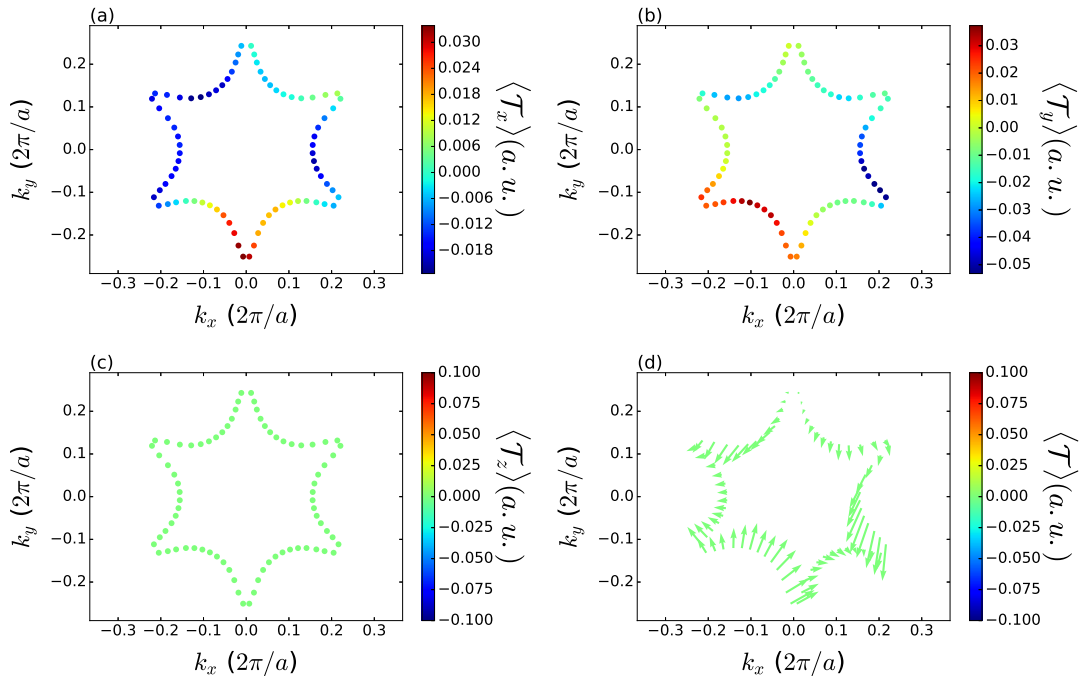


Figure 3.11: Expectation value of the x component of the torque $\langle \mathcal{T}_x \rangle$ (a), of the y component of the torque $\langle \mathcal{T}_y \rangle$ (b), and of the z component of the torque $\langle \mathcal{T}_z \rangle$ (c), for the scattering states on the Fermi surface integrated in the atomic cell of the central Mn impurity, in the case of 51 Mn impurities on the Bi_2Te_3 surface. (d) The same as in (a-c), but with the x and y components presented by arrows and the z component by a color code.

Calculating the expectation value of the spin-orbit torque for the scattering states on the Fermi surface at the central Mn atom of the system with 51 impurities, as it is shown in Fig. 3.11, we observe that they are one order of magnitude larger than the corresponding torque expectation values of the system with only one defect (Fig. 3.8). This gives a good indication of the dependency of the torque by the magnetic field. The presence of magnetic impurities on the surface Bi_2Te_3 gives rise to a larger torque.

As the magnetization of all the impurity atoms is in z direction, the z component of the torque expectation value is zero (Fig. 3.8(c)). The 120° rotation symmetry of the torque expectation values in the $x - y$ plane on the Fermi surface is broken.

As on the system with one defect, as well as on this system with 51 Mn atoms the sign of the torque expectation value $\langle \mathcal{T}_y \rangle$ follows the negative sign of the spin expectation value ($\langle -\sigma_x \rangle$), i.e. a surface state in x direction causes a spin-orbit torque which is transverse in y direction, in accordance with Eq. (2.13). Also, the sign of the torque expectation value $\langle \mathcal{T}_x \rangle$ follows the sign of the spin expectation value ($\langle \sigma_y \rangle$).

In Fig. 3.12(a-c) the components of the spin flux expectation value are presented, when Bi_2Te_3 is doped with 51 Mn impurities. As the spin and the torque operators, the spin flux operator presents no symmetry rotation. It is important to note that the spin flux expectation values $\langle -Q_x \rangle$ are practically equal to the torque expectation values $\langle \mathcal{T}_x \rangle$, as $\langle -Q_y \rangle$ are in agreement with $\langle \mathcal{T}_y \rangle$.

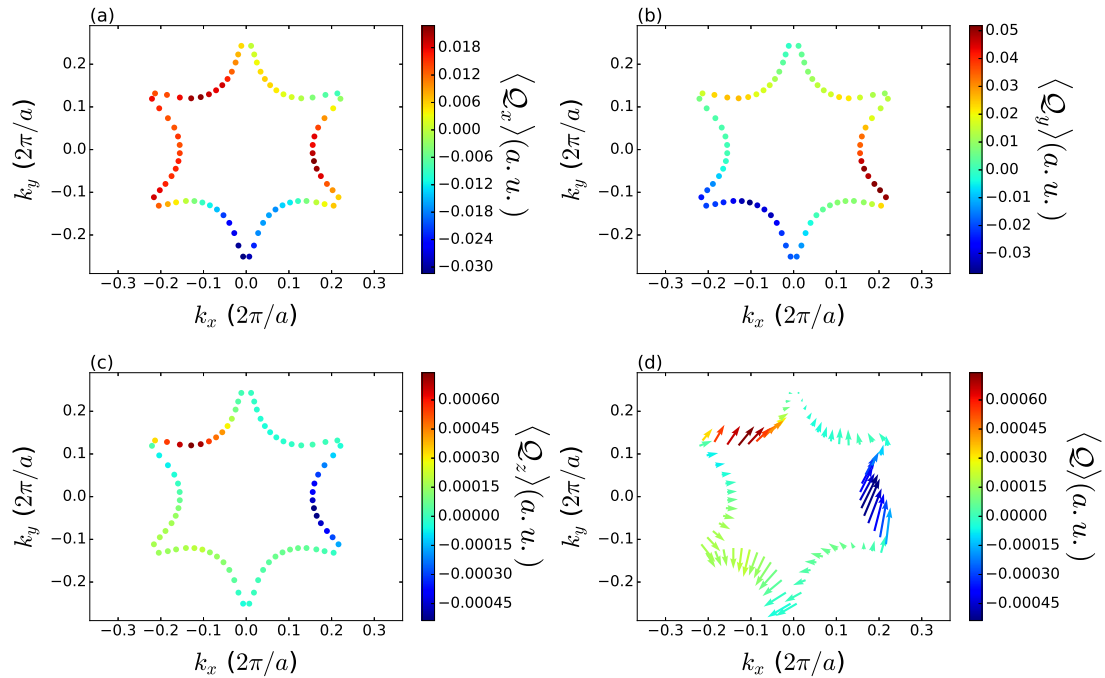


Figure 3.12: Expectation value of the x component of the spin flux $\langle Q_x \rangle$ (a), of the y component of the spin flux $\langle Q_y \rangle$ (b), and of the z component of the spin flux $\langle Q_z \rangle$ (c), for the scattering states on the Fermi surface integrated in the atomic cell of the central Mn impurity, in the case of 51 Mn impurities on the Bi_2Te_3 surface. (d) The same as in (a-c), but with the x and y components presented by arrows and the z component by a color code.

3.4 Calculations of the response tensors based on Boltzmann formalism

Applying an external electric field in the system, a current density is created, induced by the propagated waves of the crystal electrons (Bloch's electrons). The Bloch waves forming the current, are scattered of the perturbing potential of magnetic impurities, creating a wave interference in the region of impurities. In this Section we calculate the current-induced spin orbit torques in the presence of Mn impurities on the Bi_2Te_3 surface, based on the Boltzmann formalism.

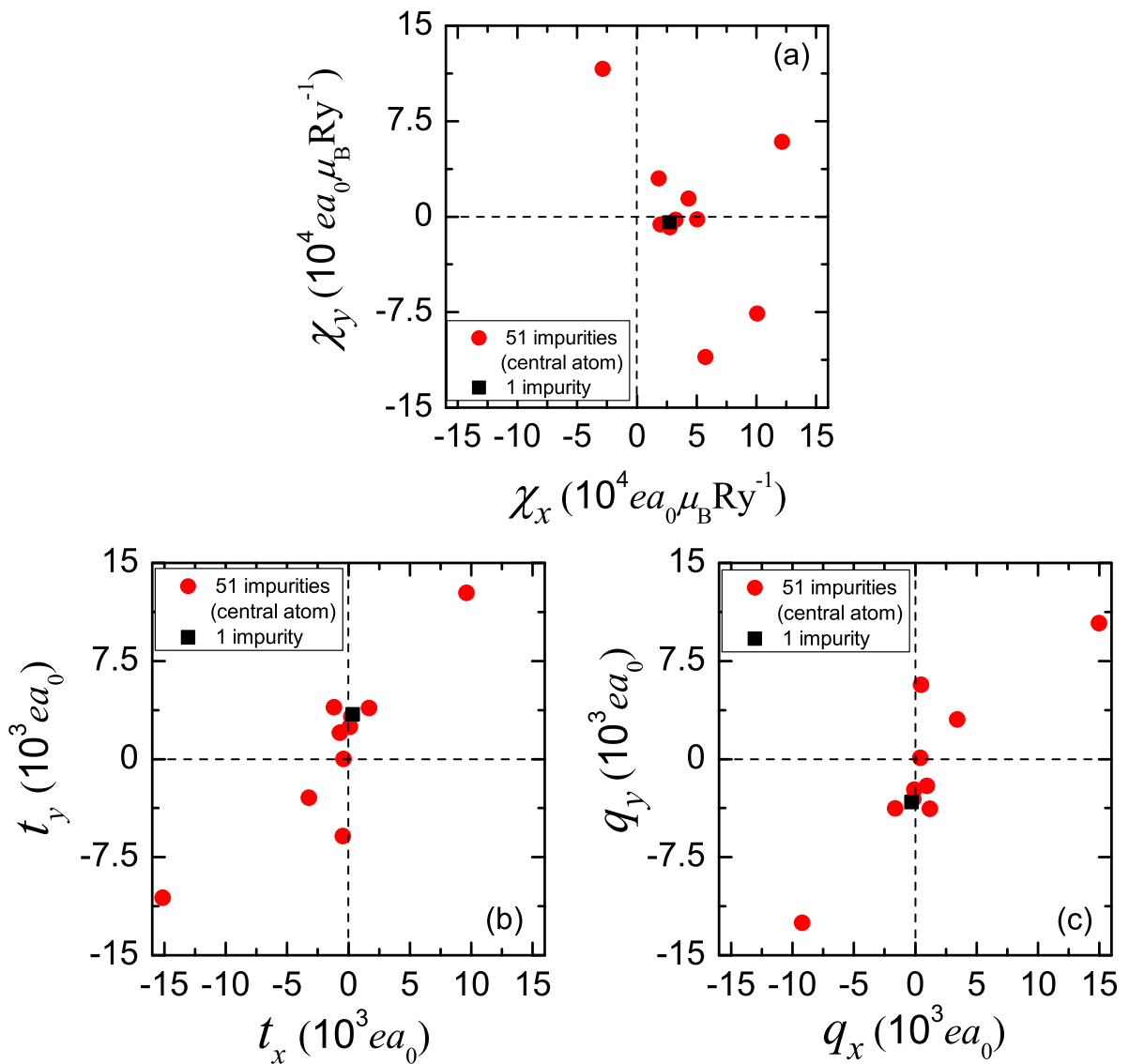


Figure 3.13: The response coefficient of (a) the spin accumulation χ_{yx} , (b) the torque t_{yx} , and (c) the spin flux q_{yx} on the central impurity atom, in the presence of 1 Mn defect (squares) and 51 Mn defects (circles) on the Bi_2Te_3 surface. The electric field (\mathcal{E}_y) is in y direction.

According to Section 2.3.2, the self-consistently calculated vector mean free path (Eq. 2.41) and the deviation of the distribution function from equilibrium, we compute the response tensors of the spin accumulation, the torque and the spin flux, in the electric field, using Eqs (2.56), (2.53) and (2.59), respectively.

The results which are presented refer to the tensor components in response to the electric field \mathcal{E}_y . The tensor components in response to the electric field \mathcal{E}_x are similar. More specifically, Figs. 3.13(a-c) represent the spin accumulation χ_{xy} , the torkance t_{xy} , and the spin flux response function q_{xy} which are exerted on the Mn impurity atom of a system with one defect, and on the central atom of a system with 51 Mn impurity atoms for the ten different distributions. We observe that the results of all response functions for the 10 different distributions present a large spread. However, we can deduce that the system with a single impurity is a representative system, as the average of the response tensors of the 10 different distributions converges to the value of the response tensor of the one impurity system ³.

As we can observe in Fig. 3.14, where the torkance as a function of the response tensor of spin accumulation is presented, there is no linear correlation between the spin of the conduction electrons and the spin-orbit torque. This absence of linear coordination is due to the external product of spin with the magnetic field, according to which the spin-orbit torque is defined (Eq. 2.6). Then, the torkance ((2.53)) does not separate into two integrals (one for the spin and one for the magnetic field), but is calculated by a convolution involving one integral which includes the external product, according to Equation (2.14).

In Fig. 3.15 the dependence of the torque response tensor by the response tensor of the spin flux is presented. The torque has a linear dependence on the spin flux, in accordance with the results of the corresponding expectation values. Consequently, the spin-orbit torque exerted on the impurity moment is essentially mediated by the spin currents in the presence of an external electric field on the system, while other contributions (in particular, the spin-lattice contribution due to the SOC inside the Mn impurity) are negligible.

Finally, comparing the results of this study to those of a ferromagnetic bilayer (a FePt/Pt thin film [35]), we find that the spin-orbit torque, in particular the torkance, is three orders of magnitude greater on Mn/Bi₂Te₃ system. As the strong spin-orbit coupling exists in both systems, this strong spin-orbit torque can be attributed to the two other main characteristics of topological insulators, i.e. to the metallic surface states combined with an insulating bulk, and to the spin direction of the conducting states into the surface. As only the surface in Bi₂Te₃ is conducting there is no current in the substrate, such as in FePt/Pt, reinforcing the spin transport on the surface states. Furthermore, on the FePt/Pt system the spin polarization of the conducting states is parallel to the magnetization of the impurity atoms, in contrast with the Mn/Bi₂Te₃, where the spin polarization is perpendicular to the magnetization of impurities.

³This should become more obvious if more distributions of impurities were included to our study.

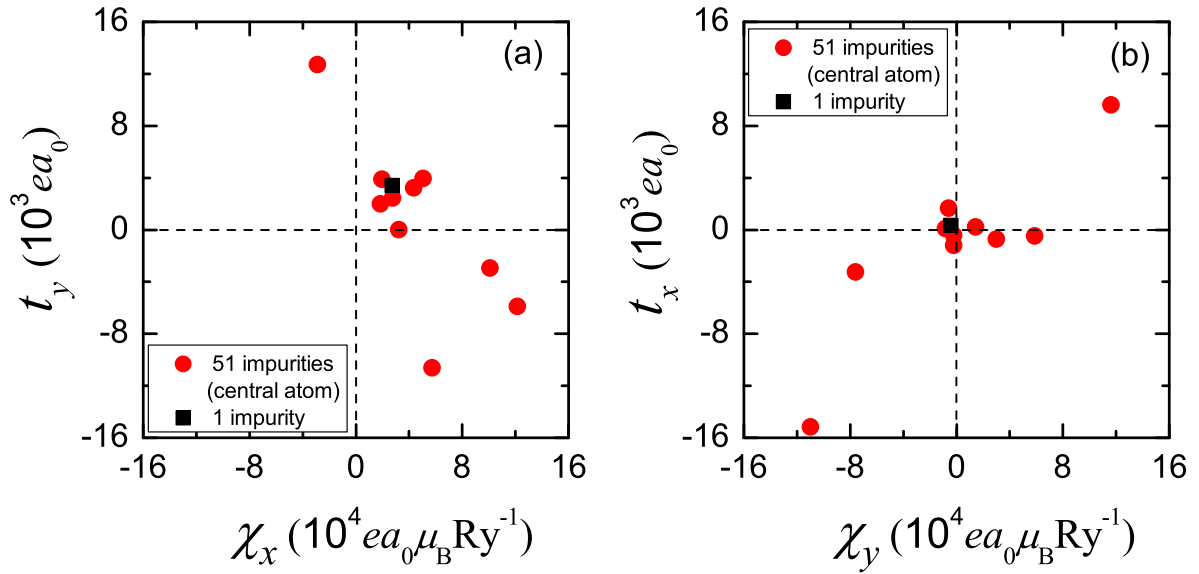


Figure 3.14: (a) The torkance t_y as a function of the response coefficient of the spin accumulation χ_x , (b) the torkance t_x as a function of the response coefficient of the spin accumulation χ_y on the central impurity atom, in the presence of 1 Mn defect (squares) and 51 Mn defects (circles) on the Bi_2Te_3 surface. The electric field (\mathcal{E}_y) is in y direction.

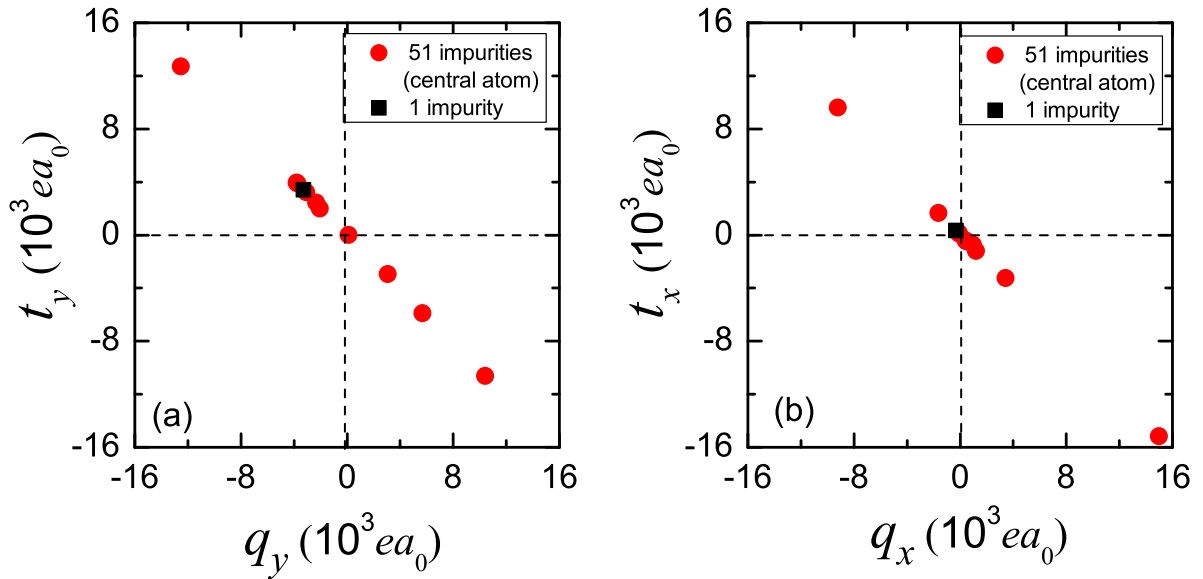


Figure 3.15: (a) The torkance t_y as a function of the response coefficient of the spin flux q_y , (b) The torkance t_x as a function of the response coefficient of the spin flux q_x on the central impurity atom, in the presence of 1 Mn defect (squares) and 51 Mn defects (circles) on the Bi_2Te_3 surface. The electric field (\mathcal{E}_y) is in y direction.

Chapter 4

Conclusion

In summary, the relativistic full potential KKR Green function method and the Boltzmann transport theory were applied to the calculations of spin-orbit torque and spin flux in Mn-doped Bi_2Te_3 surfaces.

We extracted results, studying two different approximations of the Mn/ Bi_2Te_3 system. Firstly, we investigated the case of a single Mn impurity, and then, of 51 Mn impurities, randomly placed in the area of a disk containing 1027 sites, on the Bi_2Te_3 surface. Considering, initially, the equilibrium state, we calculated the expectation value of the spin, the spin-orbit torque and the spin flux of the scattering states on the Fermi surface in the region of the Mn impurity atom. The calculated values, in the case of 51 Mn impurities are one order of magnitude larger than the corresponding results in the case of a single impurity.

Then, we investigated the non-equilibrium state, considering the application of an external electric field on the system. In particular, solving the Boltzmann equation we found the out-of equilibrium distribution function $g_{\mathbf{k}}$ in the presence of current flow. Knowing the distribution function $g_{\mathbf{k}}$, we calculated the response tensors of the spin accumulation and the spin flux in the region of the Mn impurity atom, as well as the response tensor of the spin-orbit torque exerted in the impurity moment. This was done in the case of a single impurity, as well as for a system with 51 impurities, considering 10 different distributions. In both cases the results are scaled to $\approx 5\%$ concentration. We observed that the system with a single Mn impurity gives representative values compared to the 10 different many-impurities systems. Also, we concluded that the spin-orbit torque on the impurity Mn atom is mediated by the spin flux.

Finally, we found three orders of magnitude greater torque in the Mn/ Bi_2Te_3 system, compared to a ferromagnetic bilayer (FePt/Pt) studied in the literature. Therefore, we conclude that the localized surface states and the perpendicular spin-polarization of the surface electrons, with respect to the magnetization of impurities, both characteristic of the topological insulator Bi_2Te_3 , reinforce the spin-orbit torque.

The large spin-orbit torque predicted in Mn/ Bi_2Te_3 system within this work, suggests that these systems are very promising for spintronics applications.

Appendix

In order to solve the linearized Boltzmann equation (2.42) numerically we use an iterative method. In particular, beginning with an initial guess of the vector mean free path ($\Lambda_{\mathbf{k}}^{(\text{in})}$), and replacing it on the RHS of Eq. (2.42), by solving the Boltzmann equation a new vector mean free path, $\Lambda_{\mathbf{k}}^{(\text{out})}$, is derived. If the integral of the difference between the initial and the old vector mean free path is not smaller than a selected constant, the procedure is repeated with $\Lambda_{\mathbf{k}}^{(\text{out})}$ the initial vector mean free path. In Fig. 1 we show a flow diagram of the iterative method we described above.

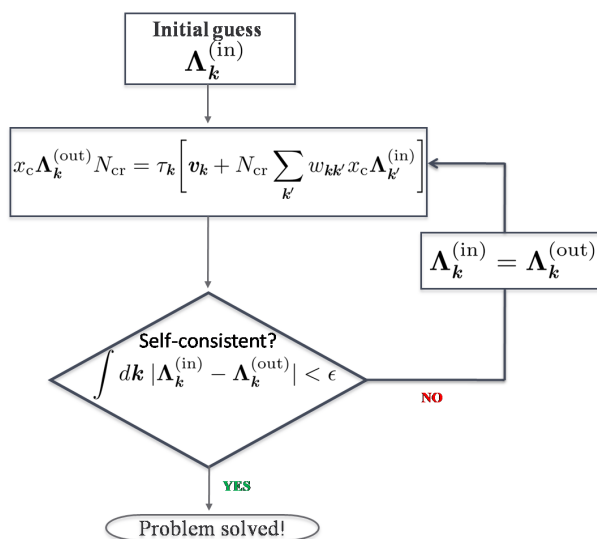


Figure 1: Flow diagram of the iterative method we apply to numerically solve the Boltzmann equation.

Bibliography

- [1] M. Z. Hasan and C. L. Kane, *Rev. Mod. Phys.* **82**, 3045 (2010).
- [2] A. Manchon and S. Zhang, *Phys. Rev. B* **79**, 094422 (2009).
- [3] I. Garate and A.H. MacDonald, *Phys. Rev. B* **80**, 134403 (2009).
- [4] F. Freimuth, S. Blügel, and Y. Mokrousov, *Phys. Rev. B* **92**, 064415 (2015).
- [5] J. Korringa, *Physica* **13**, 392 (1947).
- [6] W. Kohn and N. Rostoker, *Phys. Rev. B* **94**, 1111 (1954).
- [7] H. Ebert, D. Ködderitzsch, and J. Minar, *Rep. Prog. Phys.* **74**, 096501 (2011).
- [8] T. H. Dupree, *Ann. Phys. (N. Y.)*, **15**, 63 (1961); J. L. Beeby, *Proc. Roy. Soc. London Ser. A* **302**, 113 (1967); G. J. Morgan, *Proc. Phys. Soc.* **89**, 365 (1966).
- [9] N. Papanikolaou, R. Zeller, and P. H. Dederichs, *J. Phys.: Condens. Matter* **14**, 2799 (2002).
- [10] P. Mavropoulos and N. Papanikolaou, “The Korringa-Kohn-Rostoker (KKR) Green function method I. Electronic structure of periodic systems”, in *Computational Nanoscience: Do It Yourself!*, edited by J. Grotendorst, S. Blügel, and D. Marx, NIC Series vol **31** (John von Neumann Institute for Computing, Forschungszentrum Jülich, 2006), pp. 131-158.
- [11] D. S. G. Bauer, “Development of a relativistic full-potential first-principles multiple scattering Green function method applied to complex magnetic textures of nano structures at surfaces”, PhD thesis (RWTH Aachen, 2013).
- [12] N. H. Long, P. Mavropoulos, B. Zimmermann, D. S. G. Bauer, S. Blügel, and Y. Mokrousov, *Phys. Rev. B* **90**, 064406 (2016).
- [13] B. C. Zimmermann, “Ab initio of description of transverse transport due to impurity scattering in transition-metals”, PhD thesis (RWTH Aachen, 2014).
- [14] S. Heers, “Effect of spin-orbit scattering on transport properties of low-dimensional dilute alloys”, PhD thesis (RWTH Aachen, 2011).
- [15] P. Rießmann, “Spin scattering of topologically protected electrons at defects”, PhD thesis (RWTH Aachen, 2017).

- [16] S. Blügel, H. Akai, R. Zeller, and P. H. Dederichs, *Phys. Rev. B* **35**, 3271 (1986).
- [17] N. Stefanou, and R. Zeller, *J. Phys.: Condens. Matter* **3**, 7599 (1991).
- [18] E. N. Economou, *Greens Functions in Quantum Physics*, New York: Springer (1979).
- [19] R. Zeller, *J. Phys. C:Solid State Phys.* **20**, 2347 (1987).
- [20] G. Géranton, “Intrinsic and extrinsic spin-orbit torques from first principles ”, PhD thesis (RWTH Aachen, 2017).
- [21] F. Freimuth, S. Blügel, and Y. Mokrousov, *Phys. Rev. B* **90**, 174423 (2014).
- [22] G. Géranton, F. Freimuth, S. Blügel, and Y. Mokrousov, *Phys. Rev. B* **91**, 014417 (2015).
- [23] B. Zimmermann, P. Mavropoulos, N.H. Long, C.-R Gerhost, S. Blügel, and Y. Mokrousov, *Phys. Rev. B* **93**, 144403 (2016).
- [24] Ingrid Mertig, *Rep. Prog. Phys.* **62**, 237 (1999).
- [25] H. Ibach and H. Lüth, “An Introduction to Principles of Materials Science”, *4th Edition* (Springer, 2009).
- [26] W. Kohn and J. M. Luttinger, *Phys. Rev.* **108**, 590 (1957).
- [27] C. L. Kane, “Topological Band Theory and the \mathbb{Z}_2 invariant”, Chapter 1 in *Topological Insulators* (Elsevier, 2013).
- [28] E. Aboulouz, “Spin Scattering of Topologically Protected Electrons at Defects by the Relativistic Korringa-Kohn-Rostoker Green Function Method”, Master thesis (Universität zu Köln, 2015).
- [29] H. Zhang, C.-X. Liu, X.-L. Qi, Xi Dai, Z. Fang, and S.-C. Zhang, *Nature Physics* **5**, 438 (2009).
- [30] M. Martin, “Electronic Structure: Basic Theory and Practical Methods” (Cambridge University Press, 2004).
- [31] Y. Yavorsky, N. F. Hinsche, I. Mertig, and P. Zahn, *Phys. Rev. B* **84**, 165208 (2011).
- [32] R. Zeller, *J. Phys.: Condens. Matter* **16**, 6453 (2004).
- [33] T. Eelbo, M. Waśniowska, M. Sikora, M. Dobrzański, A. Kozowski, A. Pulkin, G. Autés, I. Miotkowski, O. V. Yazyev, and R. Wiesendanger
- [34] P. Sessi, F. Reis, T. Bathon, K. A. Kokh, O. E. Tereshchenko, and M. Bode, *Nat. Commun.* **5**, 5349 (2014).
- [35] G. Géranton, B. Zimmermann, N. H. Long, P. Mavropoulos, S. Blügel, F. Freimuth, and Y. Mokrousov, *Phys. Rev. B* **93**, 224420 (2016).